AD-A170 945 RADIATION RESISTANCE OF THIN ANTENNAS OF ARBITRARY ELEVATION AND CONFIGUR.. (U) NAVAL OCEAN SYSTEMS CENTER SAN DIEGO CA R A PAPPERT JUN 86 NOSC/TR-1112 1/1

UNCLASSIFIED F/G 9/5 NL

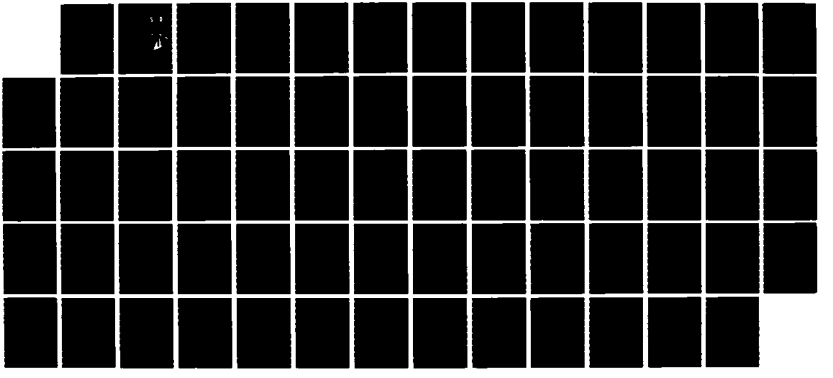

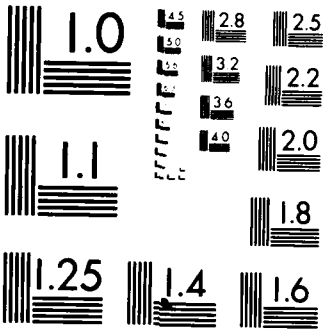

(12)

NOSC TR 1112

Technical Report 1112
June 1986
Interim Report for period
December 1985—June 1986

RADIATION RESISTANCE OF THIN ANTENNAS OF ARBITRARY ELEVATION AND CONFIGURATION OVER PERFECTLY CONDUCTING GROUND

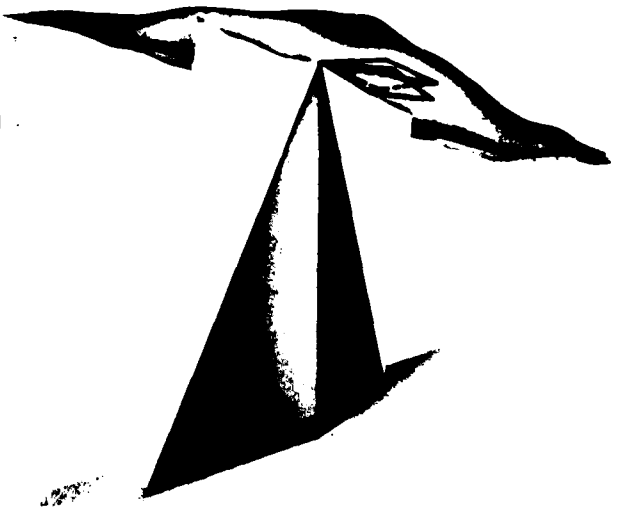

R. A. Pappert

Prepared for
Defense Nuclear Agency

Naval Ocean Systems Center
San Diego, California 92152-5000

NAVAL OCEAN SYSTEMS CENTER

San Diego, California 92152-5000

F. M. PESTORIUS, CAPT, USN
Commander

R. M. HILLYER
Technical Director

ADMINISTRATIVE INFORMATION

The work reported in this document was conducted over the period from December 1985 to June 1986 by the NOSC Modeling Branch, Code 544, for the Defense Nuclear Agency Radiation Directorate. The task was funded under DNA-RAAE program element 62715H, project number 599QMXBB.

Released by
J. A. Ferguson, Head
Modeling Branch

Under authority of
J. H. Richter, Head
Ocean and Atmospheric
Sciences Division

ACKNOWLEDGEMENTS

The author wishes to express his gratitude to Dr. P. Hansen and Mr. D. Fern for useful discussions about NEC and for providing table 1 and the current input for figure 34. The programming assistance of Ms. L. Hitney is also gratefully acknowledged.

RT

UNCLASSIFIED
SECURITY CLASSIFICATION OF THIS PAGE

AD-A170945

REPORT DOCUMENTATION PAGE

1a REPORT SECURITY CLASSIFICATION UNCLASSIFIED	1b RESTRICTIVE MARKINGS
2a SECURITY CLASSIFICATION AUTHORITY	3 DISTRIBUTION/AVAILABILITY OF REPORT Approved for public release; distribution is unlimited
2b DECLASSIFICATION/DOWNGRADING SCHEDULE	
4 PERFORMING ORGANIZATION REPORT NUMBER(S) NOSC TR 1112	5 MONITORING ORGANIZATION REPORT NUMBER(S)
6a NAME OF PERFORMING ORGANIZATION Naval Ocean Systems Center 6b OFFICE SYMBOL (If applicable) Code 544	7a NAME OF MONITORING ORGANIZATION
6c ADDRESS (City, State and ZIP Code) San Diego, CA 92152-5000	7b ADDRESS (City, State and ZIP Code)
8a NAME OF FUNDING/SPONSORING ORGANIZATION Defense Nuclear Agency Radiation Directorate 8b OFFICE SYMBOL (If applicable) DNA-RAAE	9 PROCUREMENT INSTRUMENT IDENTIFICATION NUMBER
8c ADDRESS (City, State and ZIP Code) Hybla Valley Federal Bldg Washington, DC 20305	10 SOURCE OF FUNDING NUMBERS PROGRAM ELEMENT NO: 62715H PROJECT NO: S99QMXBB TASK NO: 544-MP20 Agency Accession No.: DN651 524

11 TITLE (Include Security Classification)
Radiation Resistance of Thin Antennas of Arbitrary Elevation and Configuration Over Perfectly Conducting Ground

12 PERSONAL AUTHOR(S)
R. Pappert

13a TYPE OF REPORT	13b TIME COVERED	14 DATE OF REPORT (Year, Month, Day)	15 PAGE COUNT
Interim	FROM Dec 85 TO June 86	June 1986	60

16 SUPPLEMENTARY NOTATION

17 COSATI CODES			18 SUBJECT TERMS (Continue on reverse if necessary and identify by block number)
FIELD	GROUP	SUB GROUP	Sinusoidal current distribution Trailing-wire antennas Thin antenna radiation resistance Half-wave spiral type antennas

19 ABSTRACT (Continue on reverse if necessary and identify by block number)

Dipole segmentation is used to estimate the radiation resistance of thin antennas of arbitrary elevation and configuration over a perfectly conducting ground plane. Sample results include half-wave linear antennas of varying inclination, half-wave spiral type antennas, and a TACAMO configuration. Utility of the method for estimating the radiation resistance of VLF LF trailing-wire antennas from aircraft depends upon the extent to which the current distribution deviates from a sinusoid. That deviation is due in part to finite wire thickness as well as to the finite conductivity of both wire and ground. The influence of those effects requires further study.

20 DISTRIBUTION/AVAILABILITY OF ABSTRACT	21 ABSTRACT SECURITY CLASSIFICATION
☐ UNCLASSIFIED/UNLIMITED ☒ SAME AS RPT ☐ DTIC USERS	UNCLASSIFIED
22a NAME OF RESPONSIBLE INDIVIDUAL R. Pappert	22b TELEPHONE (Include Area Code) (619) 225-7677 22c OFFICE SYMBOL Code 544

DD FORM 1473, 84 JAN

83 APR EDITION MAY BE USED UNTIL EXHAUSTED
ALL OTHER EDITIONS ARE OBSOLETE

UNCLASSIFIED
SECURITY CLASSIFICATION OF THIS PAGE

CONTENTS

ILLUSTRATIONS

ILLUSTRATIONS (Continued)

ILLUSTRATIONS (Continued)

TABLES

1.0 INTRODUCTION

As a possible aid to improving VLF/LF modeling capability associated with trailing-wire antennas, this study examines a dipole segmentation process for rather quickly estimating the radiation resistance of thin antennas of arbitrary elevation and orientation over a perfectly conducting ground. For thin antennas, the current distribution is sinusoidal, and that distribution serves as the basis for sample calculations presented in this report. Utility of the method for estimating the radiation resistance of airborne trailing-wire systems depends upon the validity of the assumed sinusoidal current distribution. Deviations from the assumed distribution arise, in part, from the finite conductivity of the wire and ground as well as from the nonzero thickness of the antenna. A computer program that allows for such effects is the Numerical Electromagnetic Code (NEC)[1], and additional studies using this code should be made to define clearly the limitations of the present development.

In the following section, the formula for radiated power, based on dipole segmentation, is developed by integrating the Poynting flux generated by the system of radiators over a hemisphere. Although the emf method[2,3,4] may offer advantages (e.g., the method determines the complex impedance) over the direct Poynting flux integration, no attempt has been made to use that method in the present development. In Section 3, numerical results are given for half-wave linear antennas of varying inclination and for half-wave spiral type antennas.

2.0 DEVELOPMENT OF THE SEGMENTATION FORMULA

Figure 1 shows the configuration for the n^{th} dipole of current moment $\vec{M}_n$. The dipole is located at (x_n, y_n, z_n) with orientation ϕ_n and γ_n relative to the x and z axes, respectively. The field point at P has the spherical coordinates (R, θ, ϕ). A time-dependence $\exp(i\omega t)$ is assumed where $i = \sqrt{-1}$, ω is the circular frequency, and t the time. The point P is assumed to be in the far field so that the dipole field components in the θ, ϕ directions are as follows:[5]

i) Field components generated by z component of dipole.

$$E_\theta = -A_n g(R)\cos\gamma_n \sin\theta[\exp(i\psi_n^d) + R_v \exp(i\psi_n^r)] \quad (1)$$

$$H_\phi = B_n g(R)\cos\gamma_n \sin\theta[\exp(i\psi_n^d) + R_v \exp(i\psi_n^r)] \quad (2)$$

ii) Field components generated by x component of dipole.

$$E_\theta = A_n g(R)\sin\gamma_n \cos\phi_n \cos\theta\cos\phi[\exp(i\psi_n^d) - R_v \exp(i\psi_n^r)] \quad (3)$$

$$H_\phi = -B_n g(R)\sin\gamma_n \cos\phi_n \cos\theta\cos\phi[\exp(i\psi_n^d) - R_v \exp(i\psi_n^r)] \quad (4)$$

$$E_\phi = -A_n g(R)\sin\gamma_n \cos\phi_n \sin\phi[\exp(i\psi_n^d) + R_H \exp(i\psi_n^r)] \quad (5)$$

$$H_\theta = -B_n g(R)\sin\gamma_n \cos\phi_n \sin\phi[\exp(i\psi_n^d) + R_H \exp(i\psi_n^r)] \quad (6)$$

iii) Field components generated by y component of dipole.

$$E_\theta = A_n g(R)\sin\gamma_n \sin\phi_n \cos\theta \sin\phi [\exp(i\psi_n^d) - R_v \exp(i\psi_n^r)] \quad (7)$$

$$H_\phi = -B_n g(R)\sin\gamma_n \sin\phi_n \cos\theta \sin\phi [\exp(i\psi_n^d) - R_v \exp(i\psi_n^r)] \quad (8)$$

$$E_\phi = A_n g(R)\sin\gamma_n \sin\phi_n \cos\phi [\exp(i\psi_n^d) + R_H \exp(i\psi_n^r)] \quad (9)$$

$$H_\theta = B_n g(R)\sin\gamma_n \sin\phi_n \cos\phi [\exp(i\psi_n^d) + R_H \exp(i\psi_n^r)] \quad (10)$$

where

$$g(R) = \frac{e^{-ikR}}{R} \quad (11)$$

$$A_n = \sqrt{\frac{\mu_o}{\varepsilon_o}} \frac{kM_n}{4\pi i} \quad (12)$$

$$B_n = \frac{ikM_n}{4\pi} \quad (13)$$

$$\psi_n^d = k(\sin\theta\cos\phi x_n + \sin\theta\sin\phi y_n + \cos\theta z_n) \quad (14)$$

$$\psi_n^r = k(\sin\theta\cos\phi x_n + \sin\theta\sin\phi y_n - \cos\theta z_n) \quad (15)$$

k = free space wave number

R_v = Fresnel reflection coefficient for TM polarization

R_H = Fresnel reflection coefficient for TE polarizatrion.

For the special case of a perfectly conducting ground, $R_V = 1$ and $R_H = -1$. The total field components then become:

$$E_\theta = -A_n g(R)\left[g_{1n}(\theta,\phi)\exp(i\psi_n^d) + g_{2n}(\theta,\phi)\exp(i\psi_n^r)\right] \tag{16}$$

$$H_\phi = B_n g(R)\left[g_{1n}(\theta,\phi)\exp(i\psi_n^d) + g_{2n}(\theta,\phi)\exp(i\psi_n^r)\right] \tag{17}$$

$$E_\phi = -A_n g(R) g_{3n}(\theta,\phi)\left[\exp(i\psi_n^d) - \exp(i\psi_n^r)\right] \tag{18}$$

$$H_\theta = -B_n g(R) g_{3n}(\theta,\phi)\left[\exp(i\psi_n^d) - \exp(i\psi_n^r)\right] \tag{19}$$

where

$$g_{1n}(\theta,\phi) = \cos\gamma_n \sin\theta - \sin\gamma_n \cos\theta \cos(\phi-\phi_n) \tag{20}$$

$$g_{2n}(\theta,\phi) = \cos\gamma_n \sin\theta + \sin\gamma_n \cos\theta \cos(\phi-\phi_n) \tag{21}$$

$$g_{3n}(\theta,\phi) = \sin\gamma_n \sin(\phi-\phi_n) \tag{22}$$

The time average Poynting flux in the radial direction is

$$\Pi_R = \frac{1}{2}\,\mathrm{Re}\left[E_\theta H_\phi^* - E_\phi H_\theta^*\right] \tag{23}$$

where Re stands for the real part and the * for the complex conjugate. Therefore,

$$\Pi_R = -\frac{1}{2}\, g(R) g^*(R)\,\mathrm{Re}\Big\{ \sum_{n,m} A_n B_m^* \left[\exp\left(i(\psi_n^d - \psi_m^d)\right)\right](g_{1n}g_{1m} + g_{3n}g_{3m})$$

$$+ \exp(i(\psi_n^r - \psi_m^r))(g_{2n}g_{2m}+g_{3n}g_{3m})$$

$$+ \exp(i(\psi_n^d - \psi_m^r))(g_{1n}g_{2m} - g_{3n}g_{3m})$$

$$+ \exp(i(\psi_n^r - \psi_m^d))(g_{2n}g_{1m} - g_{3n}g_{3m})]\} \tag{24}$$

Now the phase terms are given by:

$$\psi_n^d - \psi_m^d = r_{nm}\sin\theta\cos(\phi - \Phi_{nm}) + z_{nm}^-\cos\theta \tag{25}$$

$$\psi_n^r - \psi_m^r = r_{nm}\sin\theta\cos(\phi - \Phi_{nm}) - z_{nm}^-\cos\theta \tag{26}$$

$$\psi_n^d - \psi_m^r = r_{nm}\sin\theta\cos(\phi - \Phi_{nm}) + z_{nm}^+\cos\theta \tag{27}$$

$$\psi_n^r - \psi_m^d = r_{nm}\sin\theta\cos(\phi - \Phi_{nm}) - z_{nm}^+\cos\theta \tag{28}$$

where

$$r_{nm} = k((x_n - x_m)^2 + (y_n - y_m)^2)^{1/2} \tag{29}$$

$$z_{nm}^- = k(z_n - z_m) \tag{30}$$

$$z_{nm}^+ = k(z_n + z_m) \tag{31}$$

$$\Phi_{nm} = \tan^{-1}\frac{y_n - y_m}{x_n - x_m} \tag{32}$$

Also,

$$g_{1n}g_{1m} = \cos\gamma_n\cos\gamma_m\sin^2\theta + \frac{1}{2}\sin\gamma_n\sin\gamma_m\cos^2\theta\cos(\phi_n-\phi_m)$$

$$- \cos\gamma_n\sin\gamma_m\sin\theta\cos\theta\cos(\phi-\phi_m) - \cos\gamma_m\sin\gamma_n\sin\theta\cos\theta\cos(\phi-\phi_n)$$

$$+ \frac{1}{2}\sin\gamma_n\sin\gamma_m\cos^2\theta\cos(2\phi-\phi_n-\phi_m) \tag{33}$$

$$g_{2n}g_{2m} = \cos\gamma_n\cos\gamma_m\sin^2\theta + \frac{1}{2}\sin\gamma_n\sin\gamma_m\cos^2\theta\cos(\phi_n-\phi_m)$$

$$+ \cos\gamma_n\sin\gamma_m\sin\theta\cos\theta\cos(\phi-\phi_m) + \cos\gamma_m\sin\gamma_n\sin\theta\cos\theta\cos(\phi-\phi_n)$$

$$+ \frac{1}{2}\sin\gamma_n\sin\gamma_m\cos^2\theta\cos(2\phi-\phi_m-\phi_n) \tag{34}$$

$$g_{1n}g_{2m} = \cos\gamma_n\cos\gamma_m\sin^2\theta - \frac{1}{2}\sin\gamma_n\sin\gamma_m\cos^2\theta\cos(\phi_n-\phi_m)$$

$$+ \cos\gamma_n\sin\gamma_m\sin\theta\cos\theta\cos(\phi-\phi_m) - \cos\gamma_m\sin\gamma_n\sin\theta\cos\theta\cos(\phi-\phi_n)$$

$$- \frac{1}{2}\sin\gamma_n\sin\gamma_m\cos^2\theta\cos(2\phi-\phi_m-\phi_n) \tag{35}$$

$$g_{2n}g_{1m} = \cos\gamma_n\cos\gamma_m\sin^2\theta - \frac{1}{2}\sin\gamma_n\sin\gamma_m\cos^2\theta\cos(\phi_n-\phi_m)$$

$$+ \cos\gamma_m\sin\gamma_n\sin\theta\cos\theta\cos(\phi-\phi_n) - \cos\gamma_n\sin\gamma_m\sin\theta\cos\theta\cos(\phi-\phi_m)$$

$$- \frac{1}{2}\sin\gamma_n\sin\gamma_m\cos^2\theta\cos(2\phi-\phi_n-\phi_m) \tag{36}$$

$$g_{3n}g_{3m} = \frac{1}{2}\sin\gamma_n\sin\gamma_m\cos(\phi_n-\phi_m) - \frac{1}{2}\sin\gamma_n\sin\gamma_m\cos(2\phi-\phi_n-\phi_m) \tag{37}$$

The time-averaged power, Pw, radiated by the system of dipoles is obtained by integrating the radial component of the time-averaged Poynting vector over the surface of a large hemisphere. Thus,

$$Pw = \lim_{R\to\infty} \left[R^2 \int_0^{\pi/2} \sin\theta d\theta \int_0^{2\pi} \Pi_R d\phi\right] \tag{38}$$

The integral over ϕ may be evaluated by using the well-known expansion[6]

$$e^{i\lambda\cos\beta} = \sum_{n=-\infty}^{\infty} i^n J_n(\lambda) e^{in\beta} \tag{39}$$

where J_n is the Bessel function of the first kind of order n. In effect, only terms with $n=0,\pm1$ and ±2 survive the ϕ integration. The result after integration over ϕ is

$$Pw = -2\pi \sum_{n,m} A_n B_m^* \int_0^{\pi} \sin\theta d\theta x$$

$$\{[\cos\gamma_n\cos\gamma_m + \tfrac{1}{2}\sin\gamma_n\sin\gamma_m\cos(\phi_n-\phi_m)]\cos(z_{nm}^- \cos\theta)J_0(r_{nm}\sin\theta)$$

$$+[\cos\gamma_n\cos\gamma_m - \tfrac{1}{2}\sin\gamma_n\sin\gamma_m\cos(\phi_n-\phi_m)]\cos(z_{nm}^+\cos\theta)J_0(r_{nm}\sin\theta)$$

$$+[-\cos\gamma_n\cos\gamma_m + \tfrac{1}{2}\sin\gamma_n\sin\gamma_m\cos(\phi_n-\phi_m)]\cos^2\theta\cos(z_{nm}^-\cos\theta)J_0(r_{nm}\sin\theta)$$

$$-[\cos\gamma_n\cos\gamma_m + \tfrac{1}{2}\sin\gamma_n\sin\gamma_m\cos(\phi_n-\phi_m)]\cos^2\theta\cos(z_{nm}^+\cos\theta)J_0(r_{nm}\sin\theta)$$

$$+\cos\gamma_n\sin\gamma_m\sin\theta\cos\theta\cos(\phi_{nm}-\phi_m)\sin(z_{nm}^-\cos\theta)J_1(r_{nm}\sin\theta)$$

$$-\cos\gamma_n \sin\gamma_m \sin\theta\cos\theta\cos(\Phi_{nm}-\phi_n)\sin(z^+_{nm}\cos\theta)J_1(r_{nm}\sin\theta)$$

$$+\cos\gamma_m \sin\gamma_n \sin\theta\cos\theta\cos(\Phi_{nm}-\phi_n)\sin(z^-_{nm}\cos\theta)J_1(r_{nm}\sin\theta)$$

$$+\cos\gamma_m \sin\gamma_n \sin\theta\cos\theta\cos(\Phi_{nm}-\phi_n)\sin(z^+_{nm}\cos\theta)J_1(r_{nm}\sin\theta)$$

$$+\frac{1}{2}\sin\gamma_n \sin\gamma_m \sin^2\theta\cos(2\Phi_{nm}-\phi_n-\phi_m)\cos(z^-_{nm}\cos\theta)J_2(r_{nm}\sin\theta)$$

$$-\frac{1}{2}\sin\gamma_n \sin\gamma_m \sin^2\theta\cos(2\Phi_{nm}-\phi_n-\phi_m)\cos(z^+_{nm}\cos\theta)J_2(r_{nm}\sin\theta)\} \quad (40)$$

The integral over theta in equation (40) may be evaluated using the following three formulas:

$$\int_0^{\frac{\pi}{2}} (\sin x)^{\upsilon+1}\cos(\beta\cos x)J_\upsilon(\alpha\sin x)dx = \sqrt{\frac{\pi}{2}}\alpha^\upsilon(\alpha^2+\beta^2)^{-1/2\upsilon-1/4}J_{\upsilon+1/2}((\alpha^2+\beta^2)^{1/2}) \quad (41)$$

$$\int_0^{\frac{\pi}{2}} (\sin x)^{\upsilon+1}\cos x\sin(\beta\cos x)J_\upsilon(\alpha\sin x)dx = \sqrt{\frac{\pi}{2}}\alpha^\upsilon\beta(\alpha^2+\beta^2)^{-1/2\upsilon-3/4}J_{\upsilon+3/2}((\alpha^2+\beta^2)^{1/2}) \quad (42)$$

$$\int_0^{\frac{\pi}{2}} (\sin x)^{\upsilon+1}\cos^2 x\cos(\beta\cos x)J_\upsilon(\alpha\sin x)dx = \sqrt{\frac{\pi}{2}}\alpha^\upsilon(\alpha^2+\beta^2)^{-1/2\upsilon-3/4}[J_{\upsilon+3/2}((\alpha^2+\beta^2)^{1/2})$$

$$-\beta^2(\alpha^2+\beta^2)^{-1/2}J_{\upsilon+5/2}((\alpha^2+\beta^2)^{1/2})] \quad (43)$$

Equation (41) is from Gradshteyn and Ryzhik[7], and equations (42) and (43) are easily obtained from equation (41). To evaluate the theta integrals in equation (40), equation (41) is used with υ = 0,2, equation (42) is used with υ = 1, and equation (43) is used with υ = o. With the understanding that

the current moment M_n is to be expressed in terms of the rms current associated with the n^{th} element, the expression for the radiated power after carrying out the theta integrations becomes

$$Pw = 30k^2 \sum_{n,m} M_n M_m$$

$$\{[\cos\gamma_n\cos\gamma_m + \frac{1}{2}\sin\gamma_n\sin\gamma_m\cos(\phi_n-\phi_m)](\omega_{nm}^-)^{-1/2}J_{1/2}(\omega_{nm}^-)$$

$$+ [\cos\gamma_n\cos\gamma_m - \frac{1}{2}\sin\gamma_n\sin\gamma_m\cos(\phi_n-\phi_m)](\omega_{nm}^+)^{-1/2}J_{1/2}(\omega_{nm}^+)$$

$$+[-\cos\gamma_n\cos\gamma_m + \frac{1}{2}\sin\gamma_n\sin\gamma_m\cos(\phi_n-\phi_m)](\omega_{nm}^-)^{-3/2}[J_{3/2}(\omega_{nm}^-)$$

$$-(z_{nm}^-)^2(\omega_{nm}^-)^{-1}J_{5/2}(\omega_{nm}^-)]$$

$$-[\cos\gamma_n\cos\gamma_m + \frac{1}{2}\sin\gamma_n\sin\gamma_m\cos(\phi_n-\phi_m)](\omega_{nm}^+)^{-3/2}[J_{3/2}(\omega_{nm}^+)$$

$$-(z_{nm}^+)^2(\omega_{nm}^+)^{-1}J_{5/2}(\omega_{nm}^+)]$$

$$+[\cos\gamma_n\sin\gamma_m\cos(\Phi_{nm}-\phi_m)z_{nm}^- + \cos\gamma_m\sin\gamma_n\cos(\Phi_{nm}-\phi_n)z_{nm}^-$$

$$+\frac{1}{2}\sin\gamma_n\sin\gamma_m\cos(2\Phi_{nm}-\phi_n-\phi_m)r_{nm}]r_{nm}(\omega_{nm}^-)^{-5/2}J_{5/2}(\omega_{nm}^-)$$

$$+[-\cos\gamma_n\sin\gamma_m\cos(\Phi_{nm}-\phi_m)z_{nm}^+ + \cos\gamma_m\sin\gamma_n\cos(\Phi_{nm}-\phi_n)z_{nm}^+$$

$$-\frac{1}{2}\sin\gamma_n\sin\gamma_m\cos(2\Phi_{nm}-\phi_n-\phi_m)r_{nm}]r_{nm}(\omega_{nm}^+)^{-5/2}J_{5/2}(\omega_{nm}^+)\} \qquad (44)$$

where

$$\omega^{\pm}_{nm} = ((z^{\pm}_{nm})^2 + r^2_{nm}))^{1/2} \tag{45}$$

$$j_\nu(x) = \sqrt{\frac{\pi}{2}} J_\nu(x) \tag{46}$$

$$J_{1/2}(x) = \sqrt{\frac{2}{\pi}} \frac{\sin x}{\sqrt{x}} \quad , \quad J_{3/2}(x) = \sqrt{\frac{2}{\pi}} \left(- \frac{\cos x}{\sqrt{x}} + \frac{\sin x}{x\sqrt{x}} \right)$$

$$J_{5/2}(x) = \frac{3}{x} J_{3/2}(x) - J_{1/2}(x) \tag{47}$$

Equation (44) gives the power radiated from an assembly of dipoles. This section will be concluded by checking the limiting case of Equation (44) for a single dipole over a perfectly conducting plane. Additional checks are given in the following section.

For a single dipole, the dipole subscripts may be omitted. Observe first that $r = 0$ so that the first four terms of Equation (44) are the only non-vanishing terms. Observe also that $\omega^- = z^- \to 0$ and that $\omega^+ = z^+ = 2kz$, where z is the height of the dipole above ground. Also, the following relationships apply:

$$x^{-1/2} j_{1/2}(x) = \frac{\sin x}{x} \xrightarrow[x \to 0]{} 1 \tag{48}$$

$$x^{-3/2} j_{3/2}(x) = \left(- \frac{\cos x}{x^2} + \frac{\sin x}{x^3}\right) \xrightarrow[x \to 0]{} \frac{1}{3} \tag{49}$$

$$x^{-5/2} j_{5/2}(x) = \left(-1 + \frac{3}{x^2}\right) \frac{\sin x}{x^3} - \frac{3\cos x}{x^4} \tag{50}$$

By using Equations (47) through (50), Equation (44) for the single-dipole case is reduced to:

$$P_w = 2\eta k^2 M^2 f(z^+, \gamma)$$

where

$$f(z^+, \gamma) = \left[1 + \frac{3}{(z^+)^3}(\sin z^+ - z^+ \cos z^+)\right]\cos^2\gamma$$

$$+ \left[1 + \frac{3}{2(z^+)^3}((1-(z^+)^2)\sin z^+ - z^+\cos z^+)\right]\sin^2\gamma \qquad (51)$$

Limiting values of $f(z^+, \gamma)$ are:

$$f(z^+, \gamma) \xrightarrow[z^+ \to \infty]{} 1 \qquad (52)$$

$$f(z^+, \gamma) \xrightarrow[z^+ \to 0]{} 2\cos^2\gamma \qquad (53)$$

In VLF/LF applications, airborne trailing-wire systems are often modeled by a single-point dipole. An often-used input to the NOSC mode-summing programs (e.g., reference 8) is the power radiated by a vertically oriented point dipole immediately above a perfectly conducting ground plane. Thus, if a point dipole at height z is used to model a trailing-wire system radiating a known power P_z, then the power, P, to be used in the waveguide program, is

$$P/P_z = 2/f(z^+, \gamma) \qquad (54)$$

However, it should still be realized that the point-dipole approximation is a questionable simplification, and that the preferred method is to model the antenna by a series of dipoles[9]. This requires, for a given radiated power, knowledge of the antenna current, and the present method is suggested as a possible way of expeditiously estimating that current, especially when the antenna is over highly conducting ground (e.g., seawater).

Because it is common practice to use the point-dipole approximation, the following section will begin with results based on Equation (54), followed by results for linear half-wave antennas, half-wave spiral type antennas, and finally for a TACAMO configuration.

3.0 RESULTS

Shown in figures 2 through 8 are results, based on Equation (54), along with the curves

$$z = (23.9/f_{kHz})z^{+} \tag{55}$$

which are parametric in the frequency, f_{kHz}, expressed in kilohertz. The individual figures are for inclinations ,γ, ranging from vertical ($\gamma = 0^0$) to horizontal ($\gamma = 90^0$) at 15° intervals. All of the curves for P/P_z approach a value of 2 (or 3 dB) for $z^{+}>>1$. As pointed out previously[10], that results simply from the fact that a dipole in free space radiates one half the energy of the dipole of the same strength situated vertically and immediately above a perfectly conducting plane. In the latter configuration, the image source reinforces the primary source. This gives rise to an effective moment which is twice the primary, or equivalent to, a radiated power which is four times that of the primary source in free space. However, the dipole over the conducting plane radiates only into a hemisphere, and, so, the net effect is the factor of two quoted above.

When $z^{+} \lesssim 1$, the power ratio, P/P_z, increases as γ increases. This occurs because the vertical component decreases and because the radiation resistance corresponding to the horizontal component decreases (the image totally negates the primary source for a horizontal dipole immediately above a perfectly conducting plane).

Figures 9 through 15 show radiation-resistance results for a half-wave linear antenna of inclinations varying from 0° (vertical) to 90° (horizontal) at 15° intervals. The horizontal axis is the dimensionless ratio of the altitude of the antennas midpoint (z_0) to wavelength. A sinusoidal current distribution is assumed, and the radiation resistance is referenced to the current maxima. The radiation resistance is normalized to the free-space half-wave dipole value of 73.1Ω.

Figure 9 shows comparisons between the results predicted from Equation (44) and exact results[11] for a half-wave vertical dipole ($\gamma = 0^0$) over a perfectly conducting ground. Results of Equation (44) are shown for 2 segments (N = 2), 5 segments (N = 5), and 20 segments (N = 20). Convergence to the exact result is evident. In particular, the 20-segment calculation differs from the exact calculation by $\lesssim 1\%$.

Figure 15 shows a comparison between the 20-segment result predicted from Equation (44) and exact (analytical) results[11] for a half-wave horizontal dipole ($\gamma = 90^0$) over a perfectly conducting plane. Again the results differ by $\lesssim 1\%$. As expected, for all orientations the results oscillate and gradually settle to the value one for $z_0/\lambda \gtrsim 1$.

As an example of a somewhat more general application of Equation (44), figures 16 through 33 show results for what has been termed here a half-wave "spiral dipole." The antenna configuration is described by the parametric equations

$$
\left.
\begin{aligned}
x/\lambda &= (R_o/\lambda)\cos\left[\frac{m}{(4R_o/\lambda)}\,\frac{(t+1)}{(1+m^2)^{1/2}}\right] \\
y/\lambda &= (R_o/\lambda)\,\sin\left[\frac{m}{(4R_o/\lambda)}\,\frac{t+1}{(1+m^2)^{1/2}}\right] \\
z/\lambda &= z_o/\lambda + \frac{1}{4(1+m^2)^{1/2}}\,t
\end{aligned}
\right\} \quad -1<t<1 \qquad (56)
$$

where $m = \tan\gamma$ and R_o is the radius of the spiral. The total rotation angle of the spiral is

$$
\psi = \frac{m}{2(R_o/\lambda)\,(1+m^2)^{1/2}} \qquad (57)
$$

Again, the current distribution is assumed sinusoidal with the radiation resistance referenced to the current maxima. Figures 16 through 21 show results for $R_o/\lambda = 0.1$, figures 22 through 27 are for $R_o/\lambda = 0.2$, and figures 28 through 33 are for $R_o/\lambda = 0.3$. At 30 kHz these values correspond to radii of 1, 2, and 3 km. Equation (57) shows that the total rotation angle increases as m increases and varies inversely with R_o. All of the figures from 16 through 33 have been generated from Equation (44) using a 20-segment approximation.

Unlike the half-wavelength linear dipole, the "spiral dipole" curves approach values for $z_o/\lambda \gtrsim 1$, less than the free space values because the spiral feature produces a loop like characterisitic to the antenna. The level approached for $z_o/\lambda > 1$ decreases as the total rotation angle ψ increases. For the same inclination angle, γ, the tighter spiral yields the lower radiation resistance.

A realistic TACAMO configuration is considered as the final example. Table 1 gives the coordinates of the end points of the segments used to model a 6,000-foot orbit configuration used by Bickel et al.[12]

Table 1. Antenna coordinates (6,000-foot orbit).

x (km)	y (km)	z (km)
-0.275	0.000	1.844
-0.200	-0.175	2.312
-0.689	-0.275	2.937
0.094	-0.350	3.609
0.269	-0.350	4.172
0.469	-0.288	4.750
0.688	-0.125	5.312
0.862	0.181	5.859
0.925	0.575	6.234
0.825	1.000	6.656
0.594	1.425	7.062
0.212	1.737	7.250
0.000	1.862	7.344
0.010	1.862	7.347
0.604	1.750	7.347

Figure 34 shows the radiation resistance calculated from Equation (44) using both a sinusoidal current distribution and the current distribution taken from a NEC program output[13] at 19.8 kHz for the antenna configuration of table 1 above a perfectly conducting ground. In this case, $z_o = (z_b + z_t)/2$, where z_b is the z coordinate of the bottom of the antenna, and z_t is the coordinate of the top of the antenna. For the configuration of table 1, z_o =

4.595 km and $z_0/\lambda = 0.303$. The results exhibit the same shape but differ by about 3%. Somewhat surprisingly, the NEC current distribution (which has both in-phase and quadrature components whose ratio slowly varies over the antenna) yields the higher radiation resistance. That may be due, at least partly, to the fact that the NEC current output did not include the precise current maximum (all resistances given here are presumed referenced to the current maximum). At any rate, the agreement is sufficiently encouraging to warrant further comparisons with NEC. In particular, the influence of finite wire diameter, as well as the influence of the finite conductivity of the wire and ground, should be pursued.

Exclusive of the counterpoise, coordinate extremes of which are given by the last two row entries in table 1, the total rotation angle, ψ, of the TACAMO antenna is 3.77 Radians. It is interesting to note that the result for the spiral antenna for $R_0/\lambda = 0.1$, $\gamma = 45^0$ (figure 18) corresponds to a total rotation angle $\psi = 3.53$ Radians. Though differing in detail, a decided resemblance exists between the TACAMO result and that of figure 18.

4.0 CONCLUSIONS

A dipole-segmentation formula has been developed for estimating the radiation resistance of thin antennas of arbitrary elevation and configuration over a perfectly conducting ground plane. The formula yields good agreement with the known results for linear-vertical and horizontal half-wave dipoles over a perfectly conducting ground plane. As an illustration of more general configurations, results have been given for half-wave spiral type antennas, as well as for a TACAMO configuration. Preliminary comparison of results for the latter case, with output from the NEC code, indicates a 3% discrepancy. Additional comparisons with NEC should be made with particular emphasis on determining the influence of wire thickness, as well as the influence of the finite conductivity of the antenna wire and of the ground.

5.0 REFERENCES

1. Burke, G. J. and A. J. Poggio, Numerical Electromagnetic Code (NEC) - Method of Moments, NOSC-TD 116, prepared by Lawrence Livermore Laboratory for the Naval Ocean Systems Center and Air Force Weapons Laboratory, July 1977.

2. King, R. W. P., The theory of linear antennas, Harvard University Press, Cambridge, Mass., 1956.

3. Wait, J. R., Possible influence of the ionosphere on the impedance of a ground-based antenna, J. Res. NBS 66D (Radio Prop.), No. 5, 563-569, 1962.

4. Vogler, L. E. and J. L. Noble, Curves of input impedance change due to ground for dipole antennas, NBS Monograph 72, Jan. 1964.

5. Norton, K. A., The physical reality of space and surface waves in the radiation field of radio antennas, Proc. IRE, 25, 1192-1202, 1937.

6. Stratton, J. A., Electromagnetic Theory, McGraw-Hill, Inc., New York, New York, 1941.

7. Gradshteyn, I. S. and Ryzhik, Table of Integrals, Series and Products, 4th edition, Academic Press, New York, New York, 1965.

8. Ferguson, J. A. and D. G. Morfitt, WKB mode summing program for dipole antennas of arbitrary orientation and elevation for VLF/LF propagation, NOSC TR-697, interim report prepared for the Defense Nuclear Agency, Oct. 1981.

9. Pappert, R.A. and L. R. Shockey, WKB mode summing program for VLF/ELF antennas of arbitrary length, shape and elevation, NELC interim report 713, prepared for the Defense Atomic Support Agency, June 1971.

10. Pappert, R. A. and J. E. Bickel, Vertical and horizontal VLF fields excited by dipoles of arbitrary orientation and elevation, Radio Science 5 (12), 1445-1452, 1970.

11. Kraus, J. D., Antennas, McGraw-Hill Book Co., Inc., New York, New York, 1950.

12. Bickel, J. E., D. G. Morfitt, I. J. Rothmuller and W. F. Moler, Propagation analysis of diversity for VLF communication systems, NELC TD 139, Sept. 1971.

13. Fern, D., private communication.

ILLUSTRATIONS

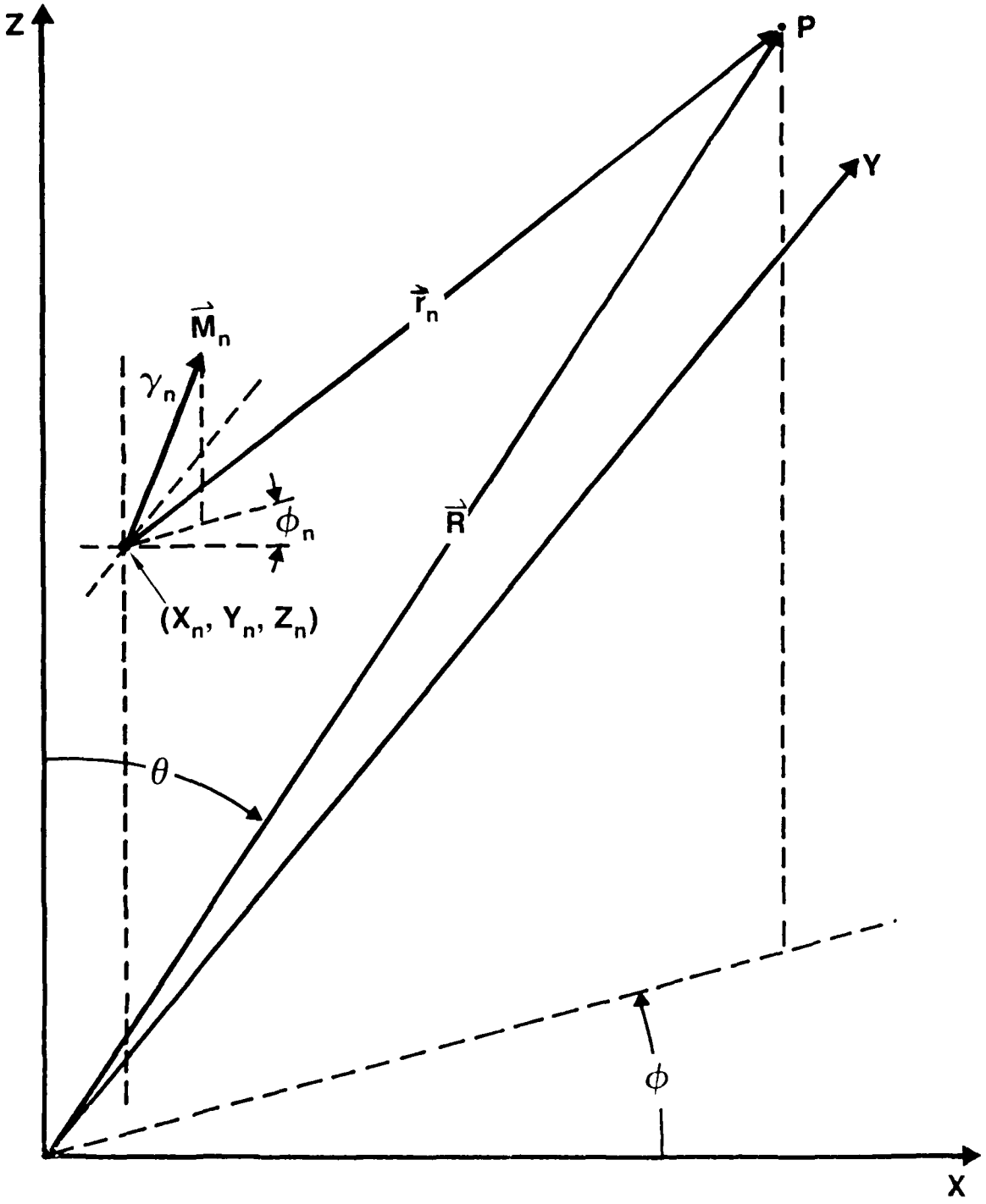

Figure 1. Dipole geometry.

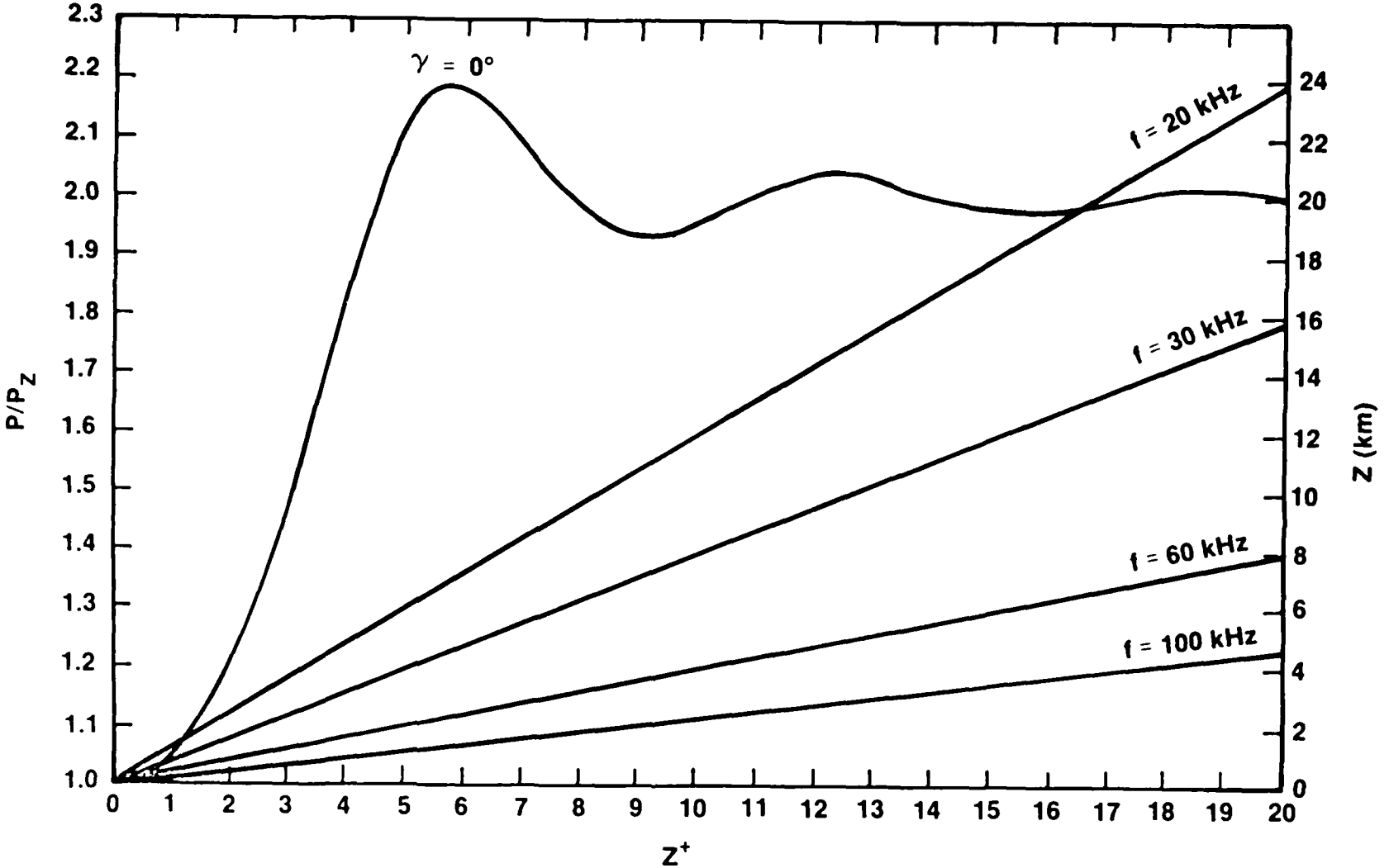

Figure 2. Power ratio (Eq. 54) for point dipole versus $z^+ = 2kz$ where z is the dipole height. Vertically oriented.

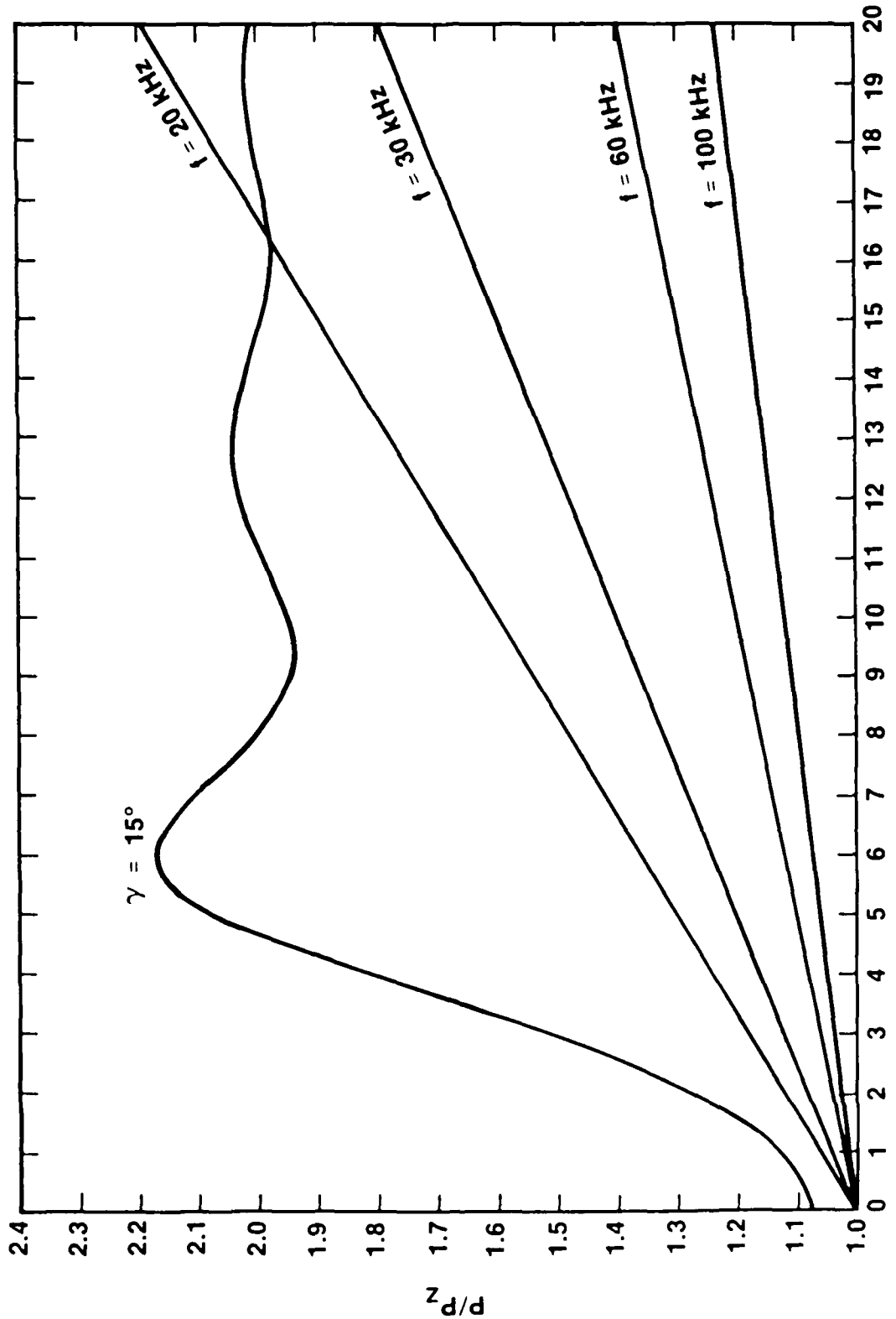

Figure 3. Power ratio (Eq. 54) for point dipole versus $z^+ = 2kz$ where z is the dipole height. Inclined 15° from vertical.

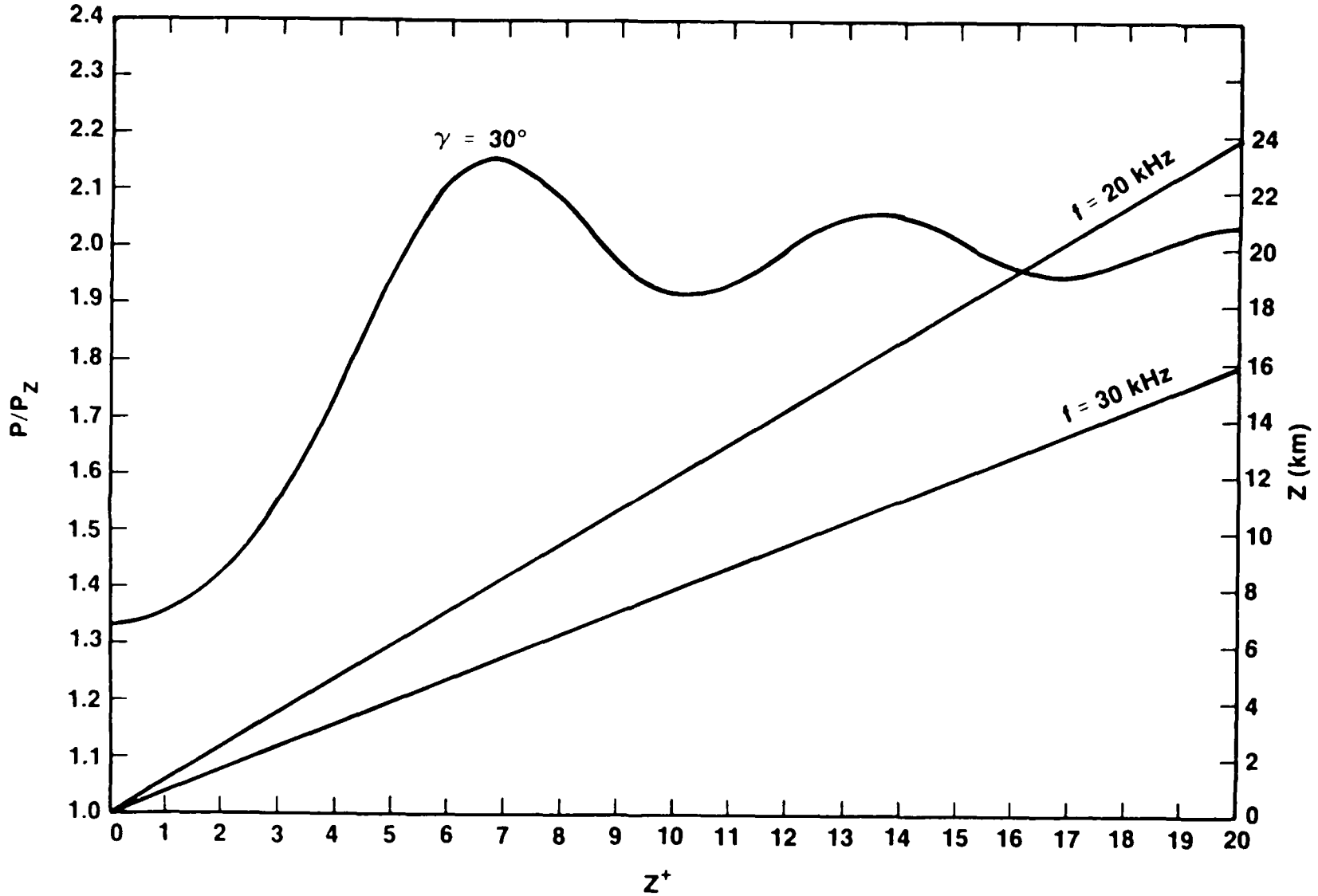

Figure 4. Power ratio (Eq. 54) for point dipole versus $z^+ = 2kz$ where z is the dipole height. Inclined 30° from vertical.

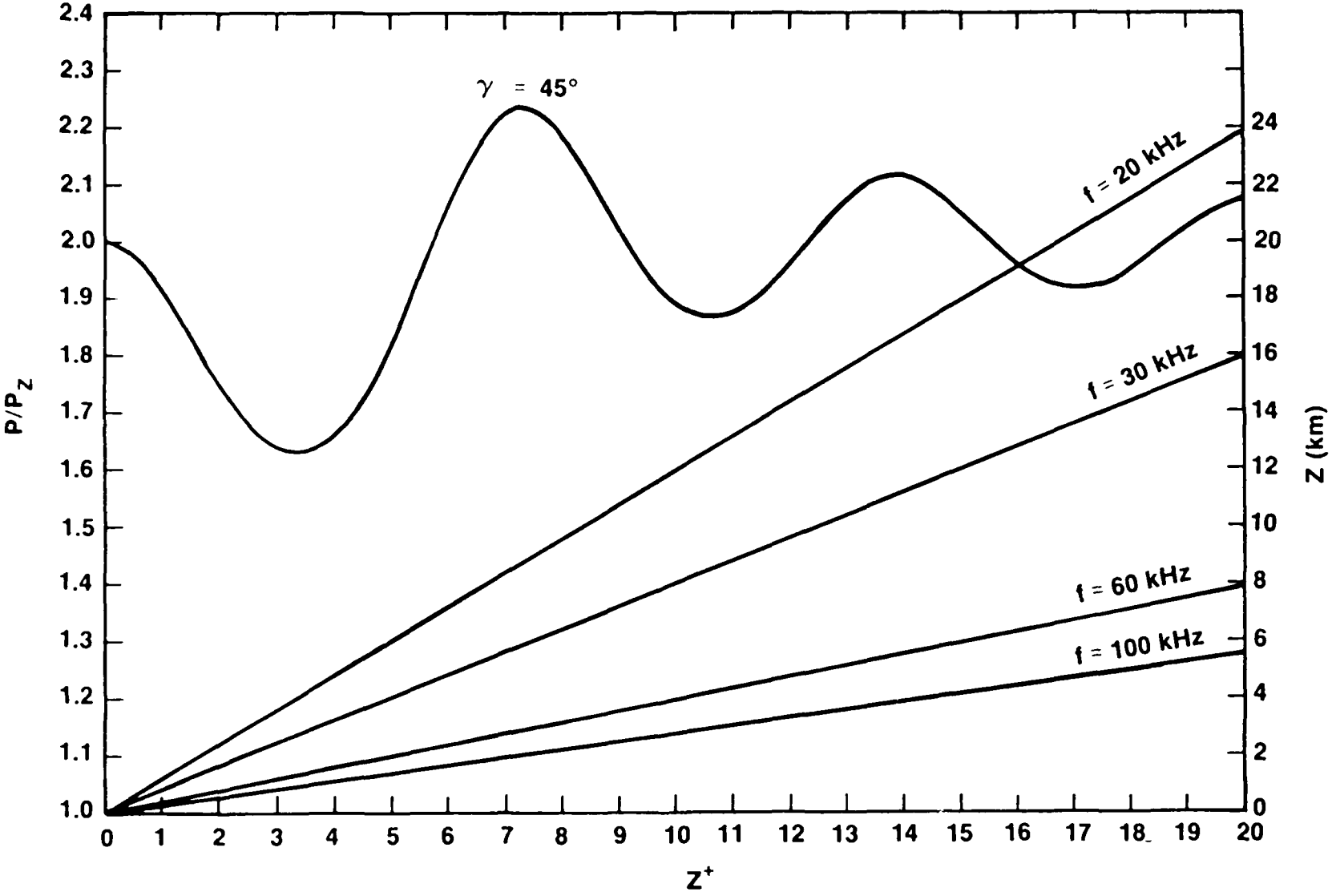

Figure 5. Power ratio (Eq. 54) for point dipole versus $z^+ = 2kz$ where z is the dipole height. Inclined 45° from vertical.

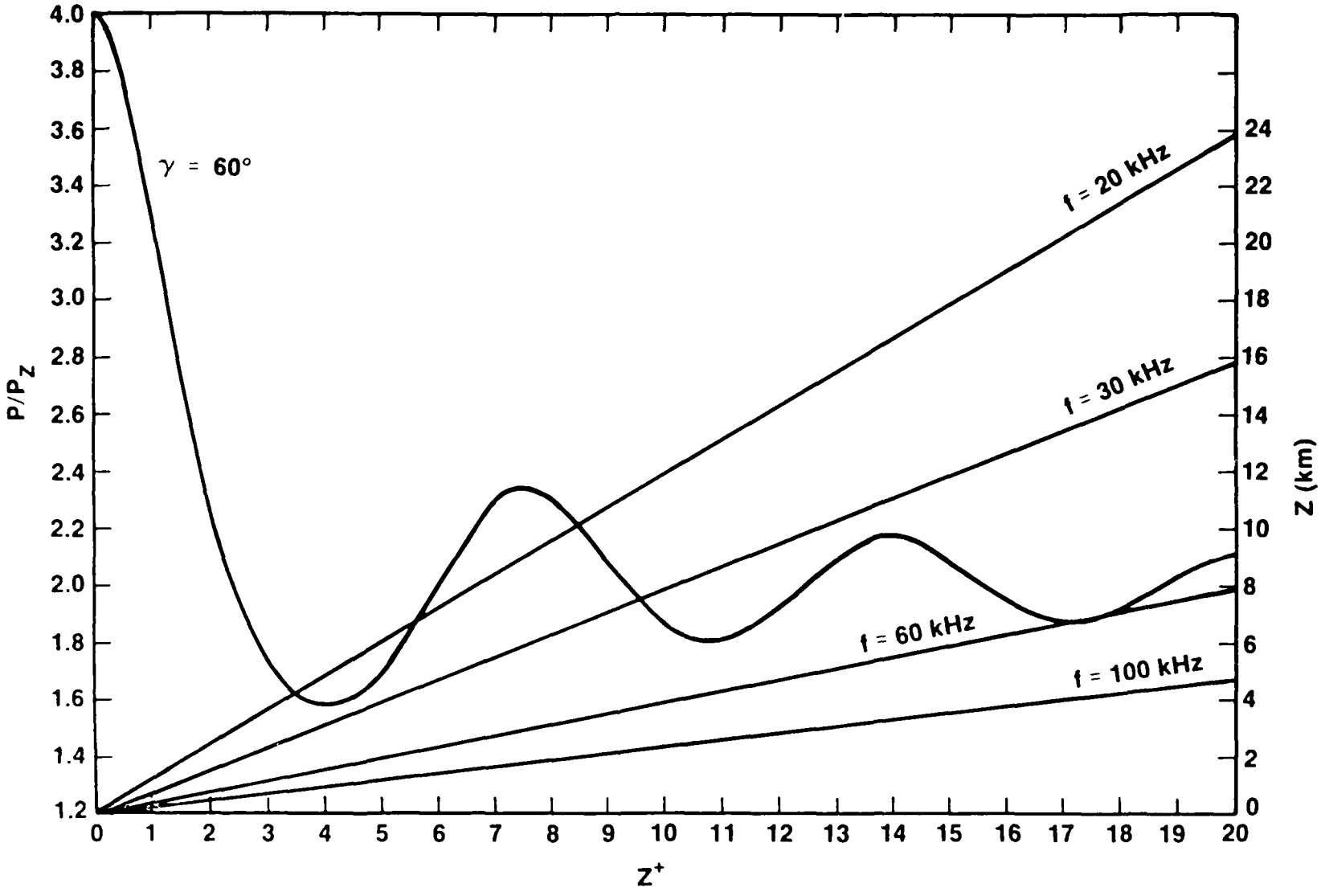

Figure 6. Power ratio (Eq. 54) for point dipole versus $z^+ = 2kz$ where z is the dipole height. Inclined 60° from vertical.

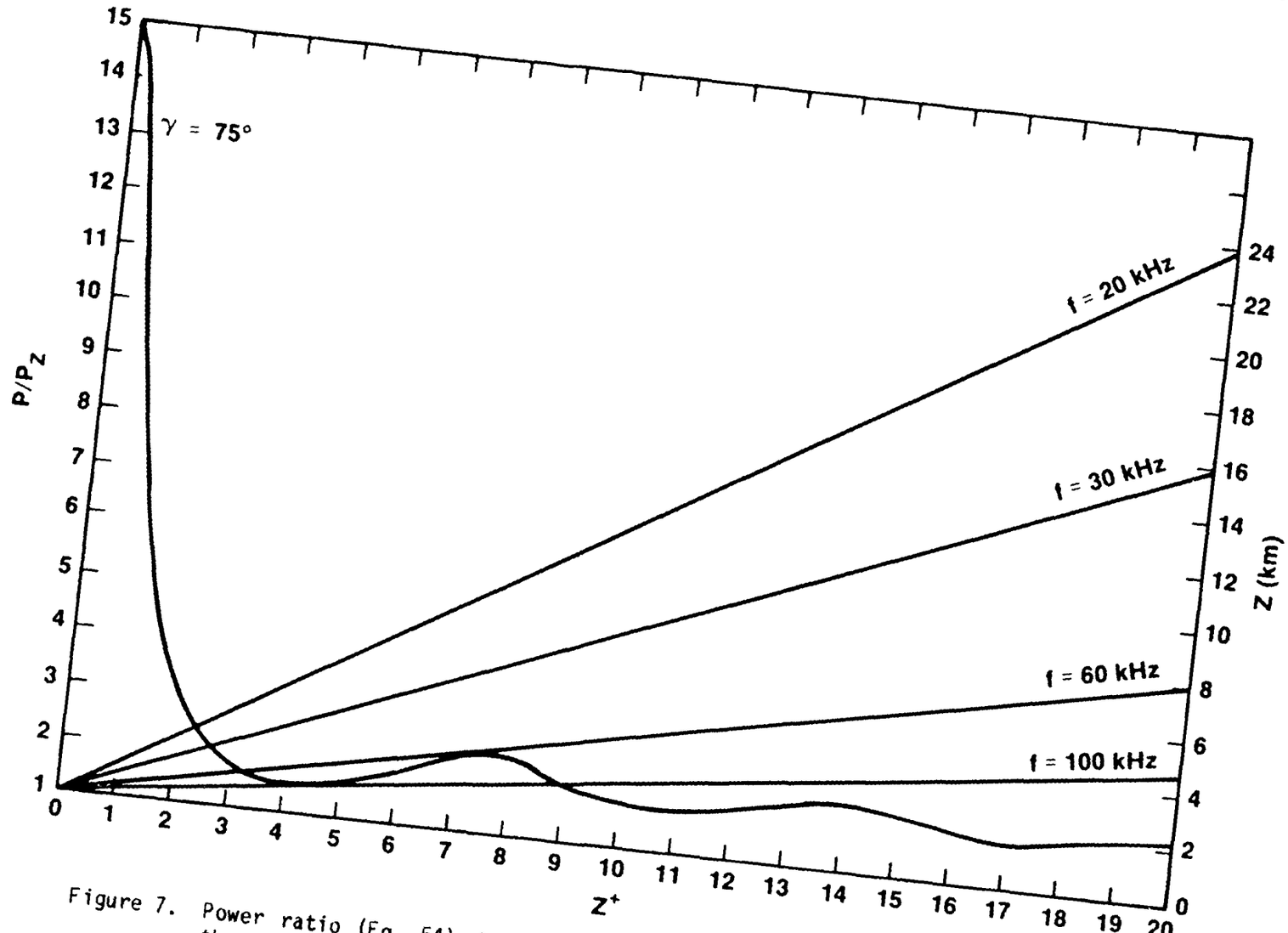

Figure 7. Power ratio (Eq. 54) for point dipole versus $z^+ = 2kz$ where z is the dipole height. Inclined 75° from vertical.

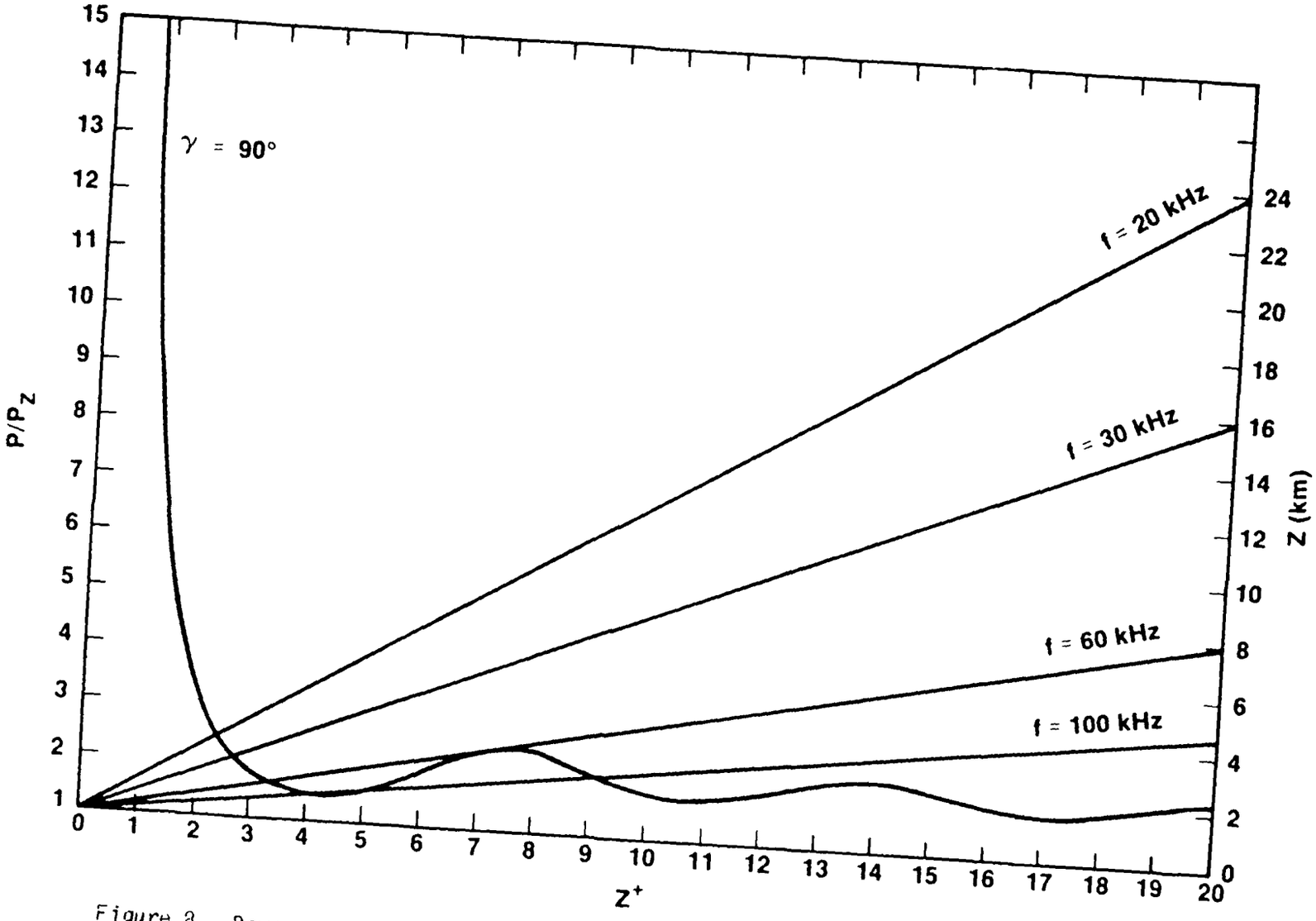

Figure 8. Power ratio (Eq. 54) for point dipole versus $z^+ = 2kz$ where z is the dipole height. Horizontally oriented.

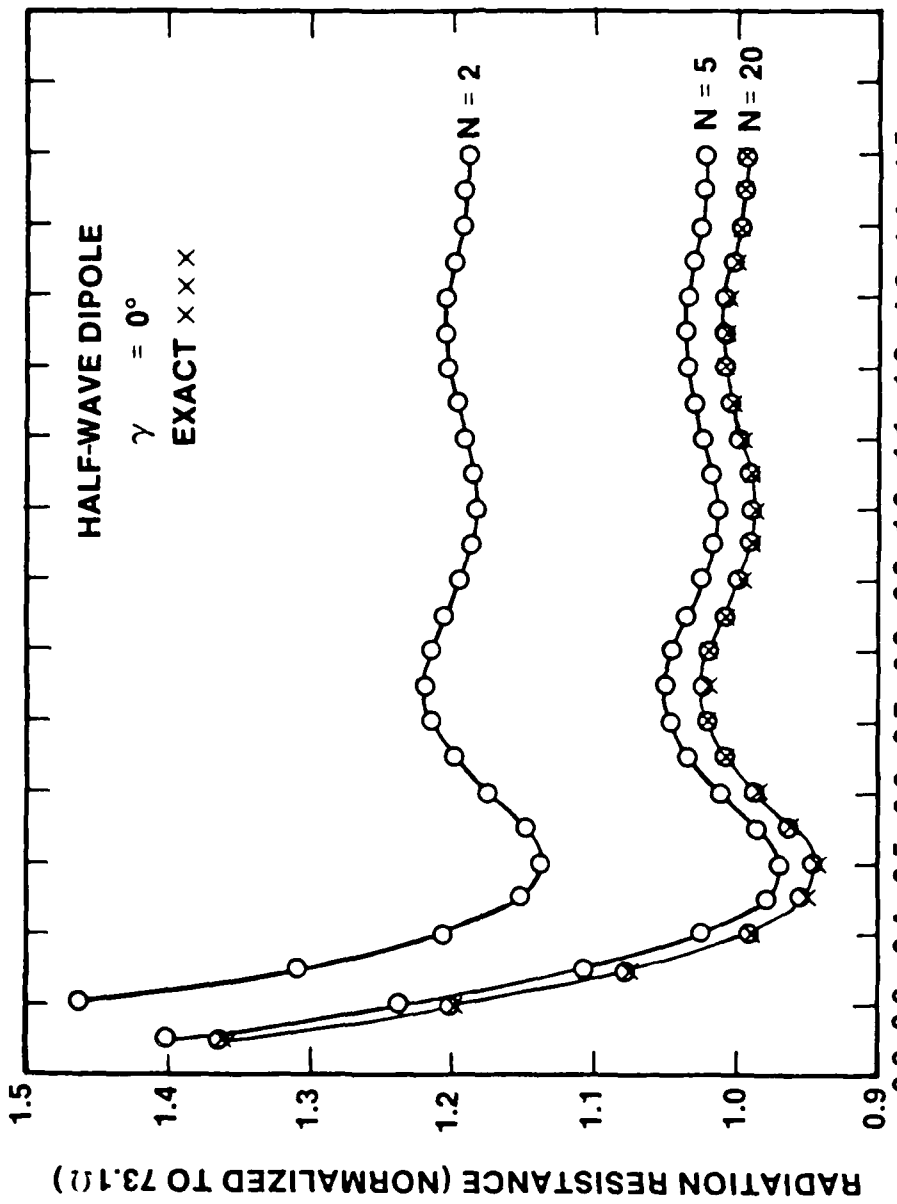

Figure 9. Normalized radiation resistance for linear half-wave dipole versus its normalized center height. Vertically oriented.

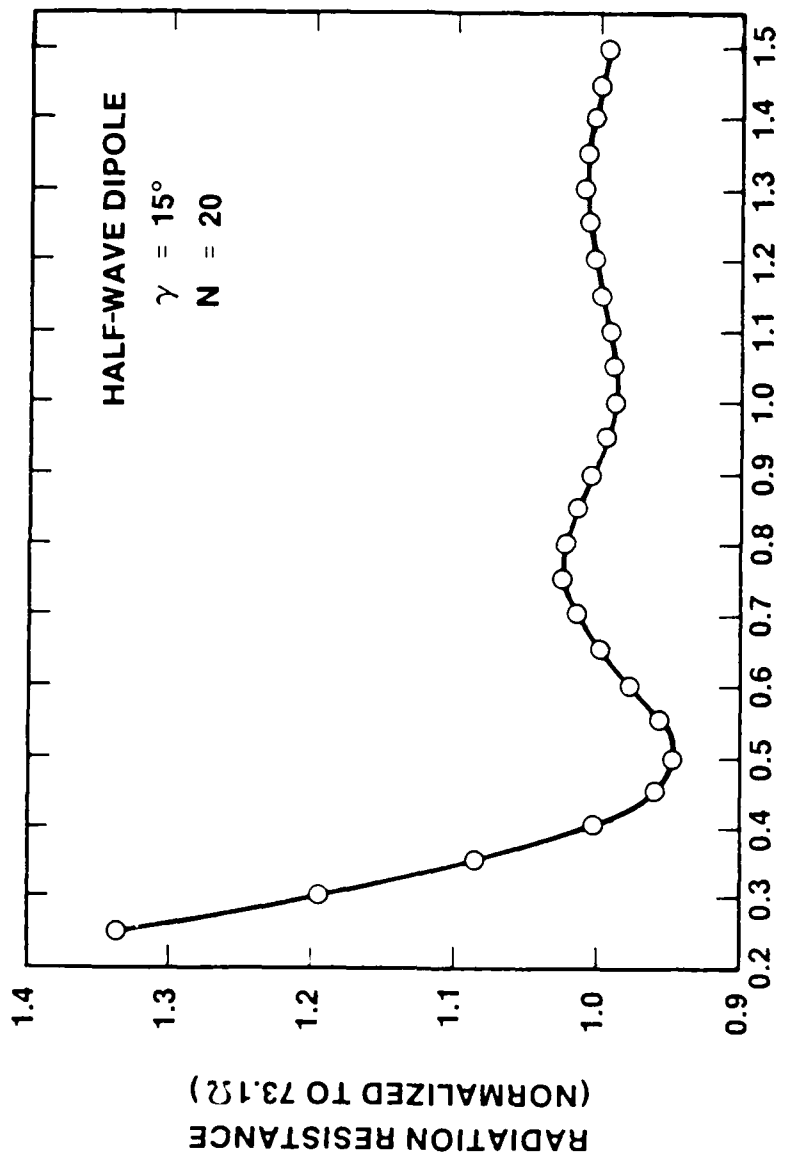

Figure 10. Normalized radiation resistance for linear half-wave dipole versus its normalized center height. Inclined 15° from vertical.

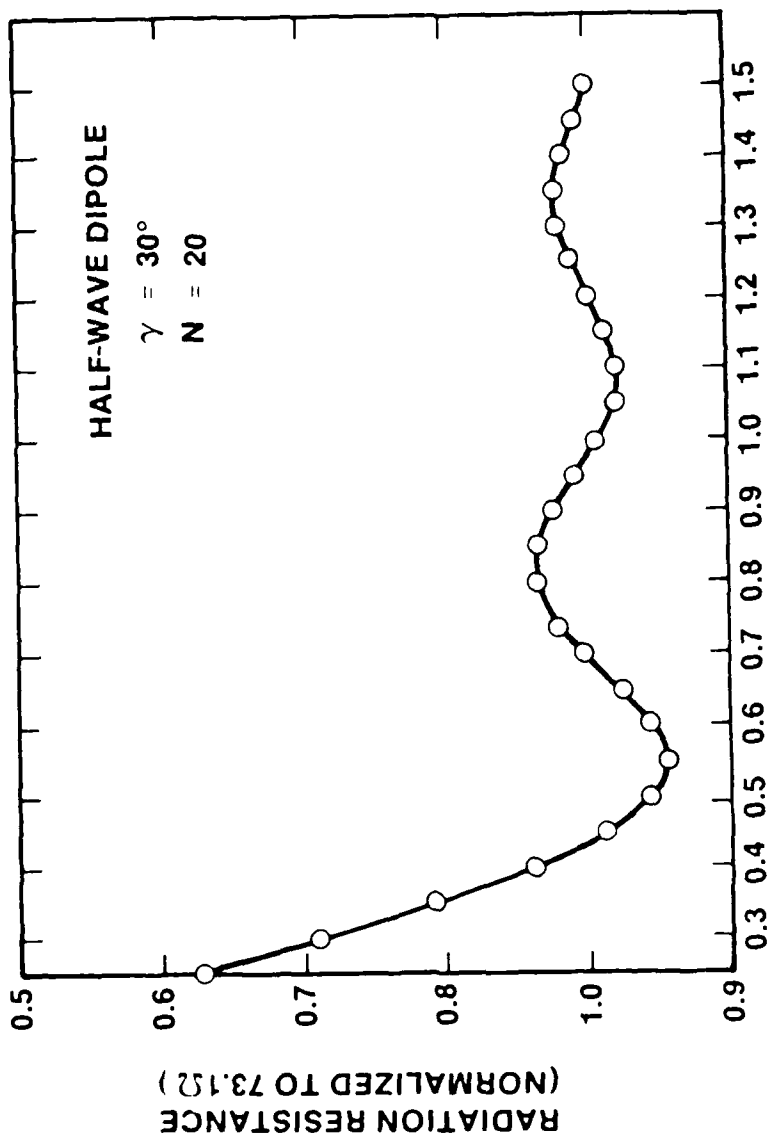

Figure 11. Normalized radiation resistance for linear half-wave dipole versus its normalized center height. Inclined 30° from vertical.

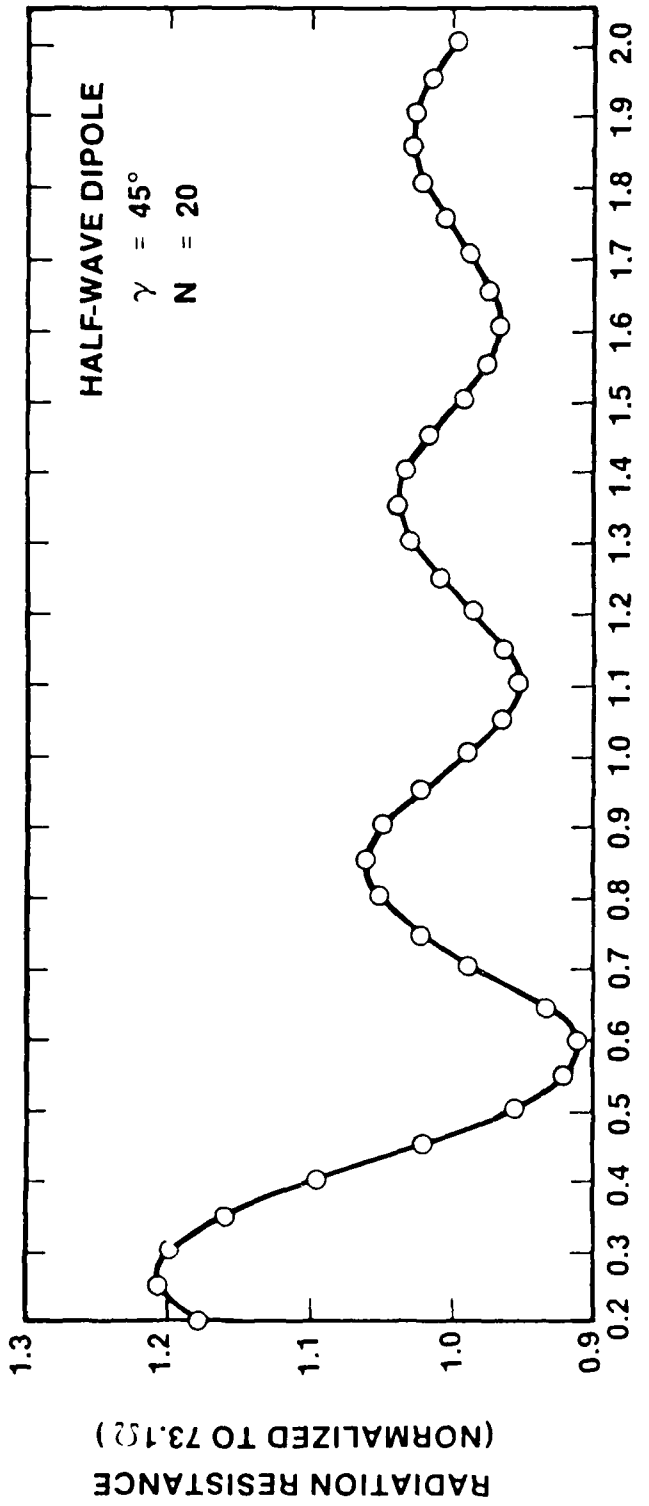

Figure 12. Normalized radiation resistance for linear half-wave dipole versus its normalized center height. Inclined 45° from vertical.

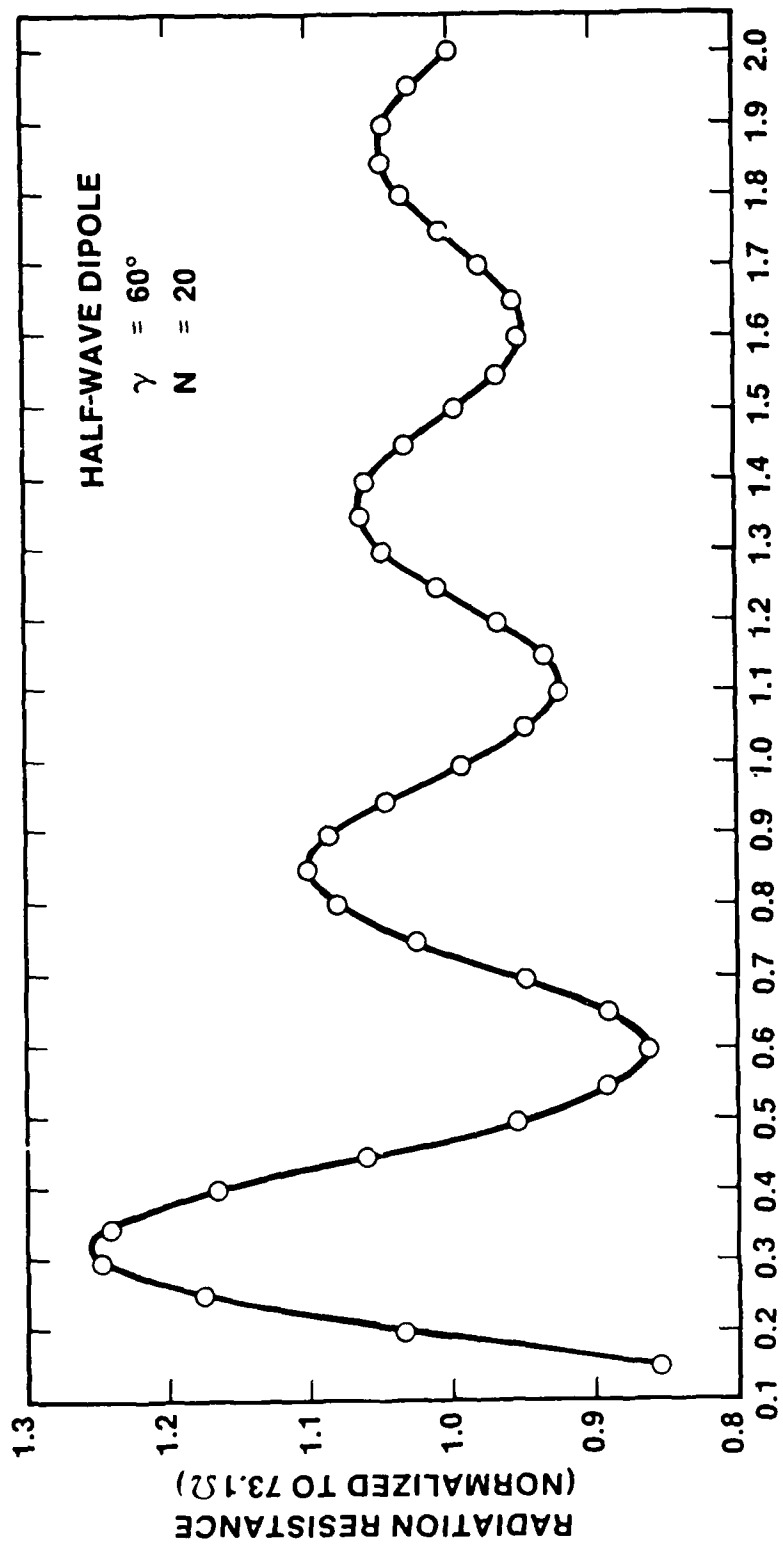

Figure 13. Normalized radiation resistance for linear half-wave dipole versus its normalized center height. Inclined 60° from vertical.

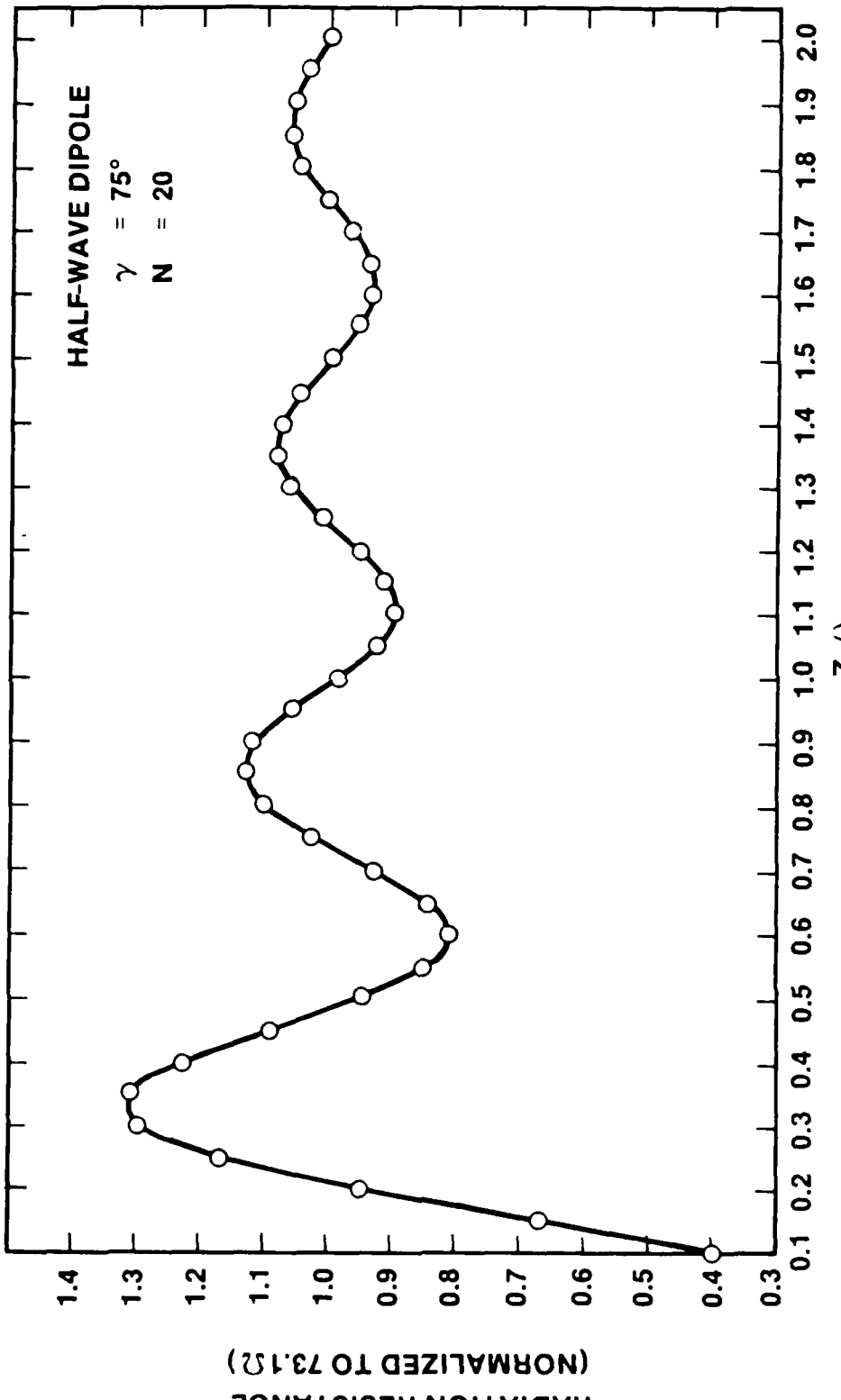

Figure 14. Normalized radiation resistance for linear half-wave dipole versus its normalized center height. Inclined 75° from vertical.

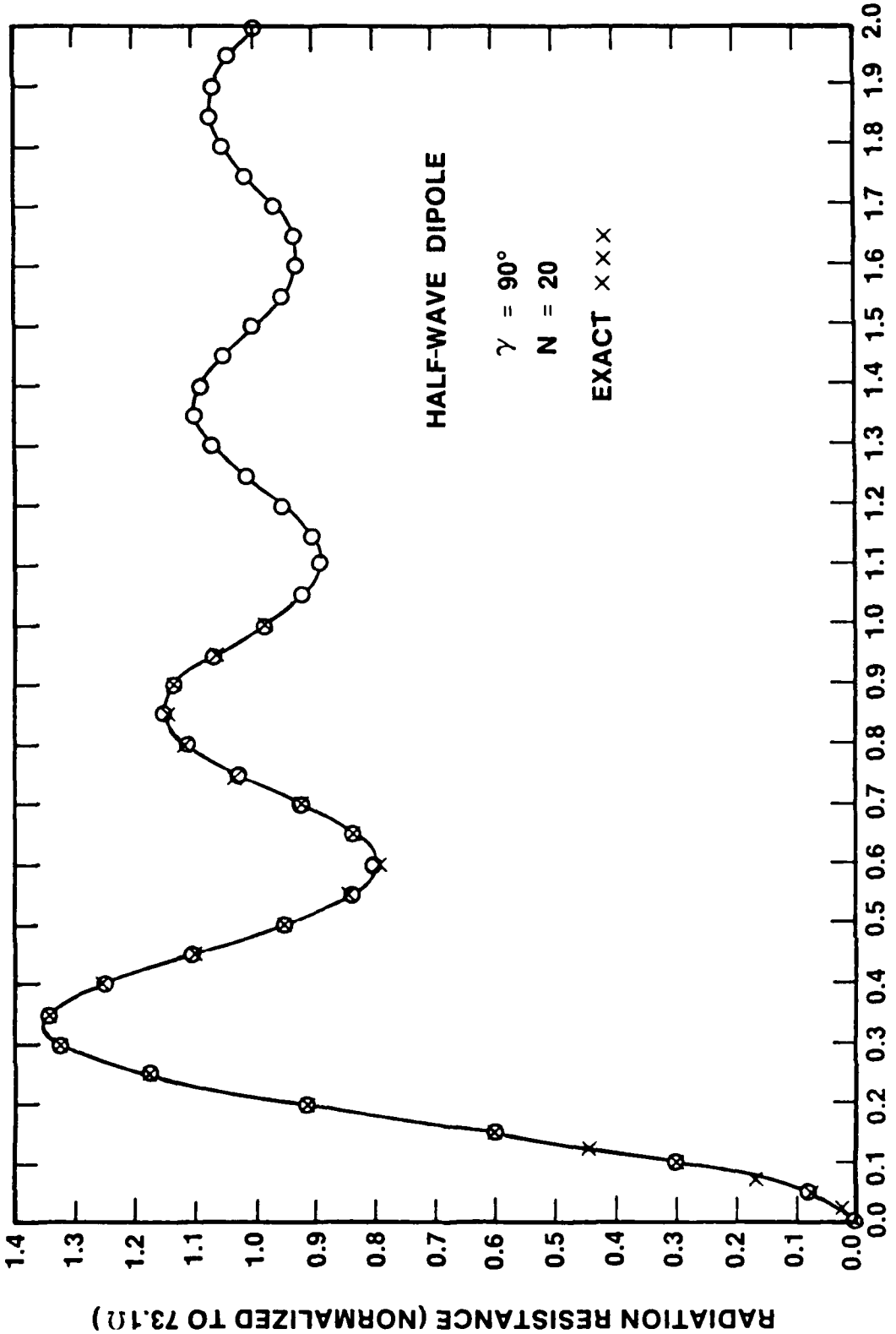

Figure 15. Normalized radiation resistance for linear half-wave dipole versus its normalized center height. Horizontally oriented.

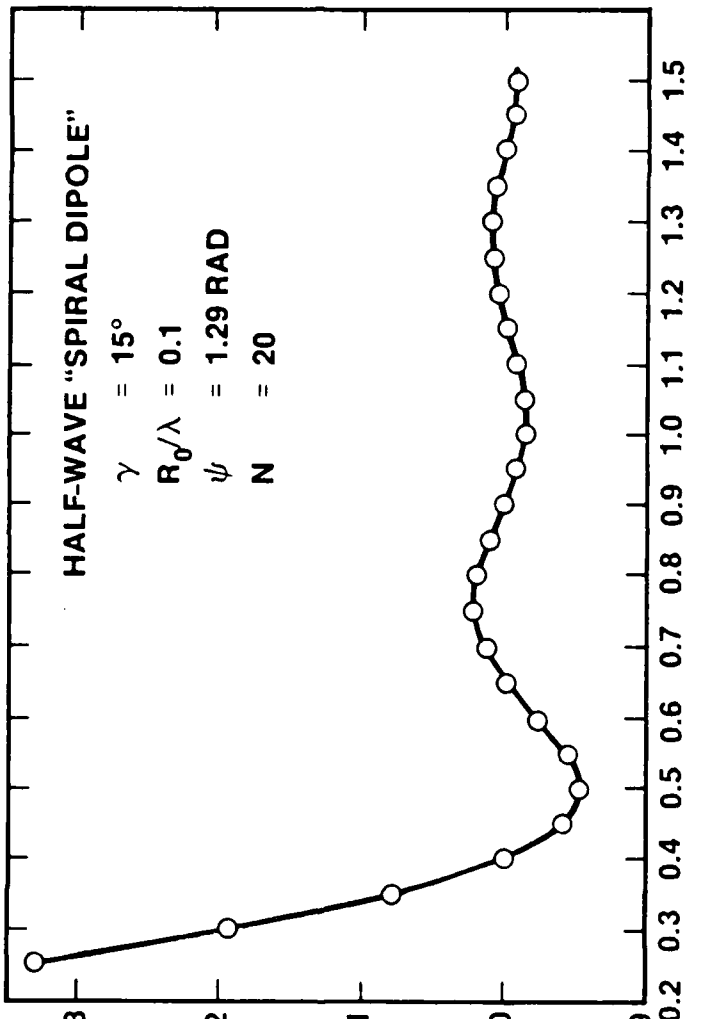

Figure 16. Normalized radiation resistance for half-wave spiral type dipole versus its normalized center height. Inclined 15° from vertical. R_0/λ - 0.1.

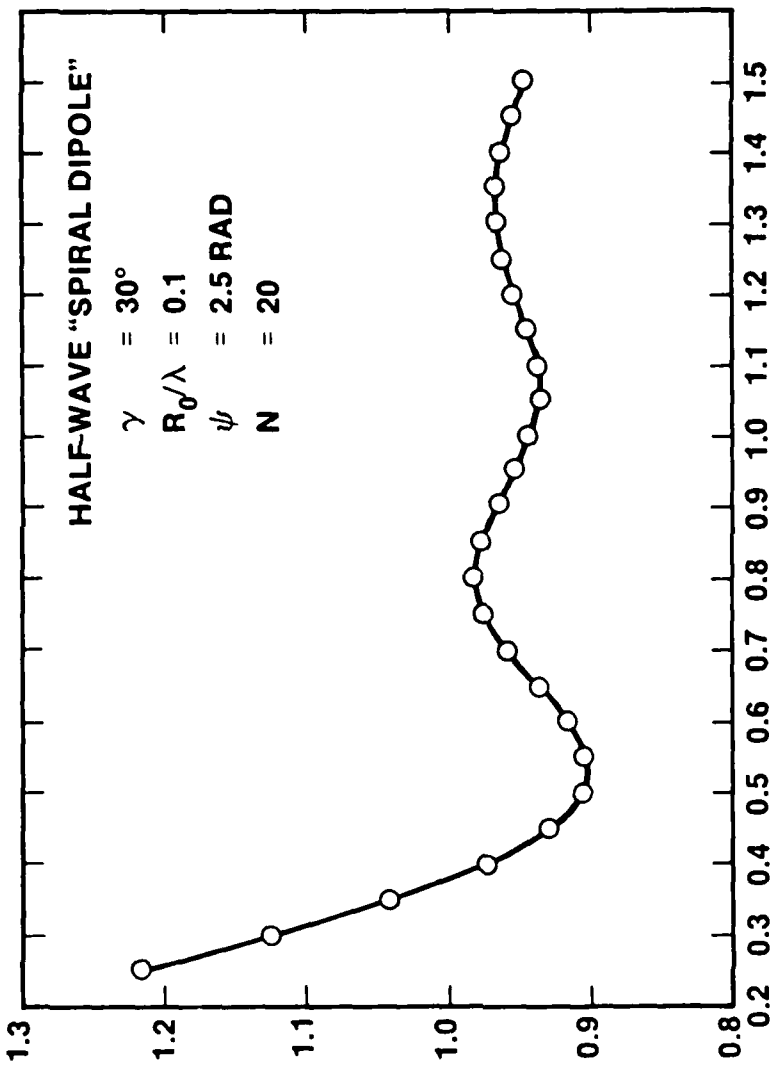

Figure 17. Normalized radiation resistance for half-wave spiral type dipole versus its normalized center height. Inclined 30° from vertical. $R_0/\lambda = 0.1$.

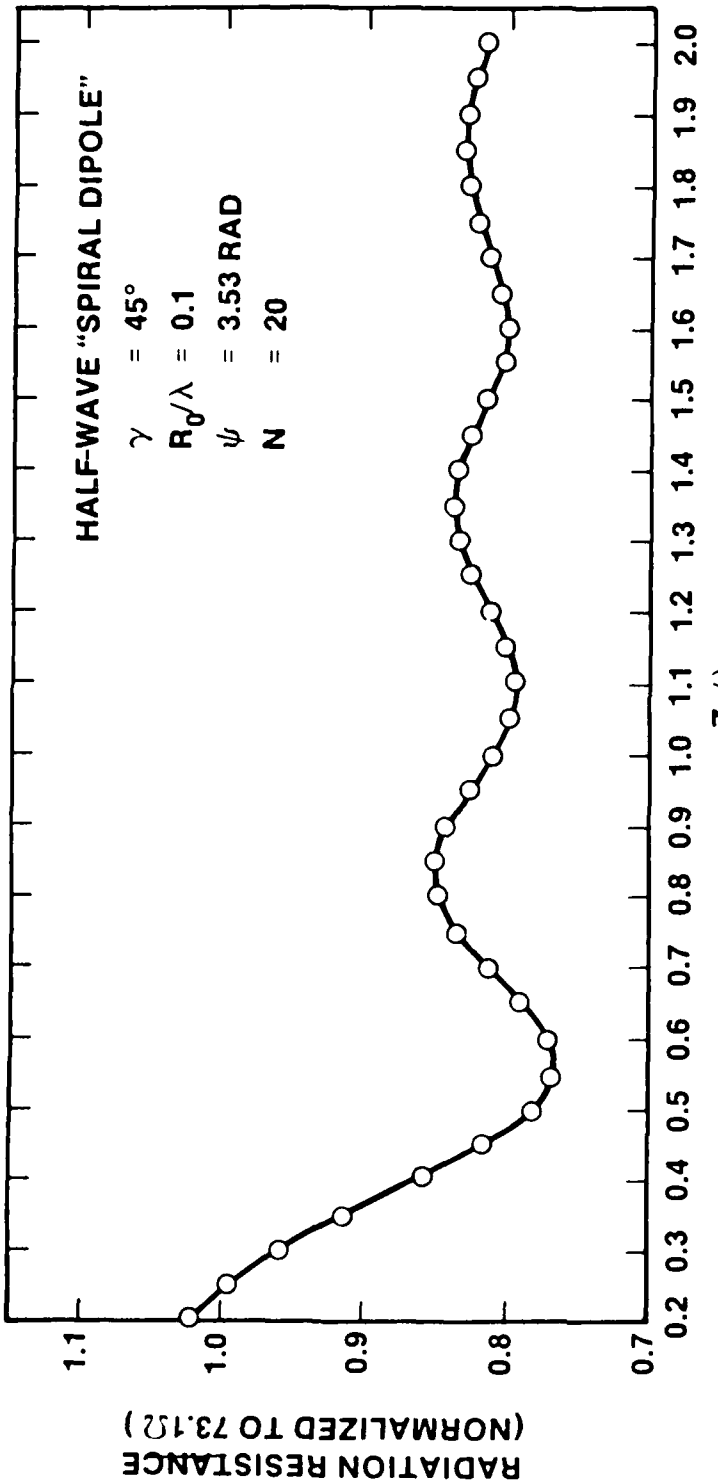

Figure 18. Normalized radiation resistance for half-wave spiral type dipole versus its normalized center height. Inclined 45° from vertical. $R_0/\lambda = 0.1$.

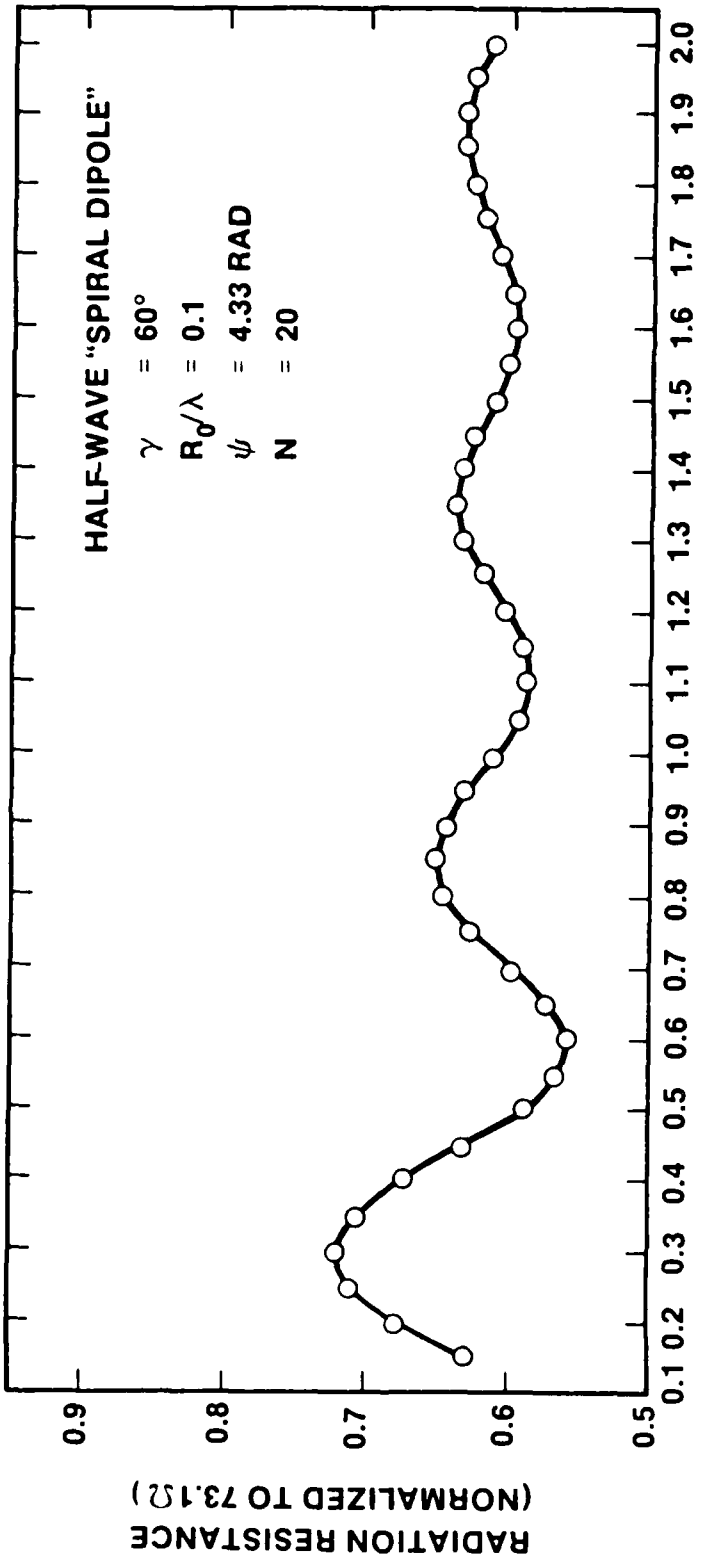

Figure 19. Normalized radiation resistance for half-wave spiral type dipole versus its normalized center height. Inclined 60° from vertical. $R_0/\lambda = 0.1$.

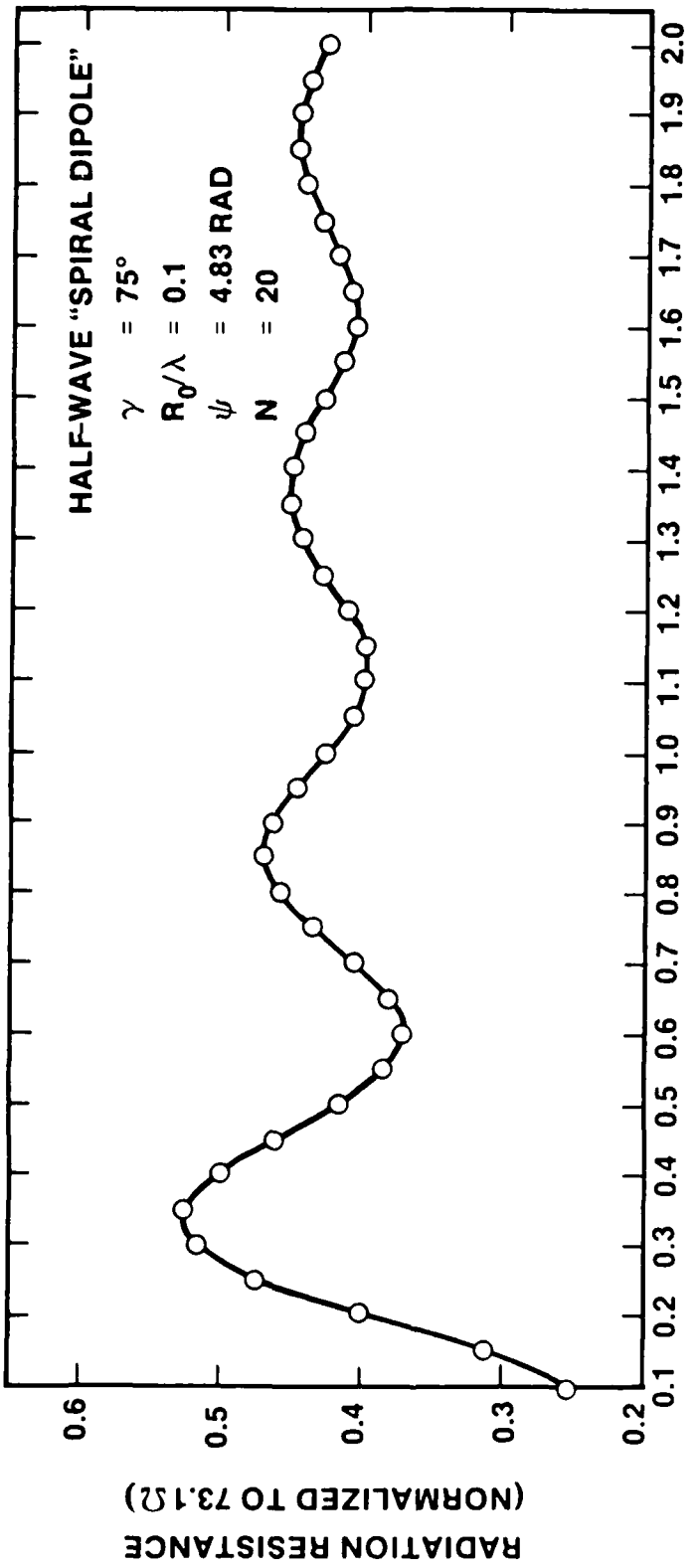

Figure 20. Normalized radiation resistance for half-wave spiral type dipole versus its normalized center height. Inclined 75° from vertical. $R_0/\lambda = 0.1$.

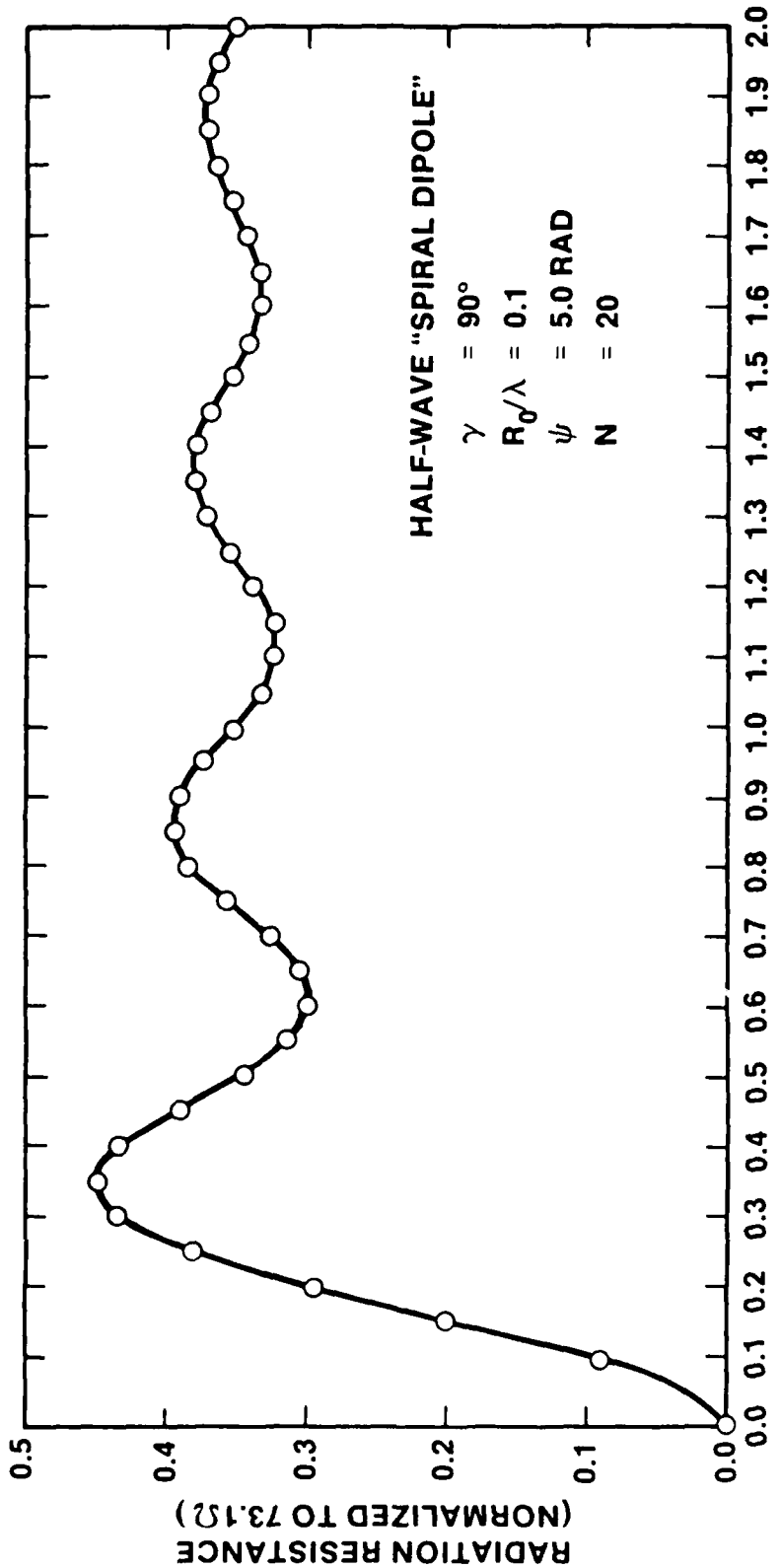

Figure 21. Normalized radiation resistance for half-wave spiral type dipole versus its normalized center height. Partial horizontal loop. $R_0/\lambda = 0.1$.

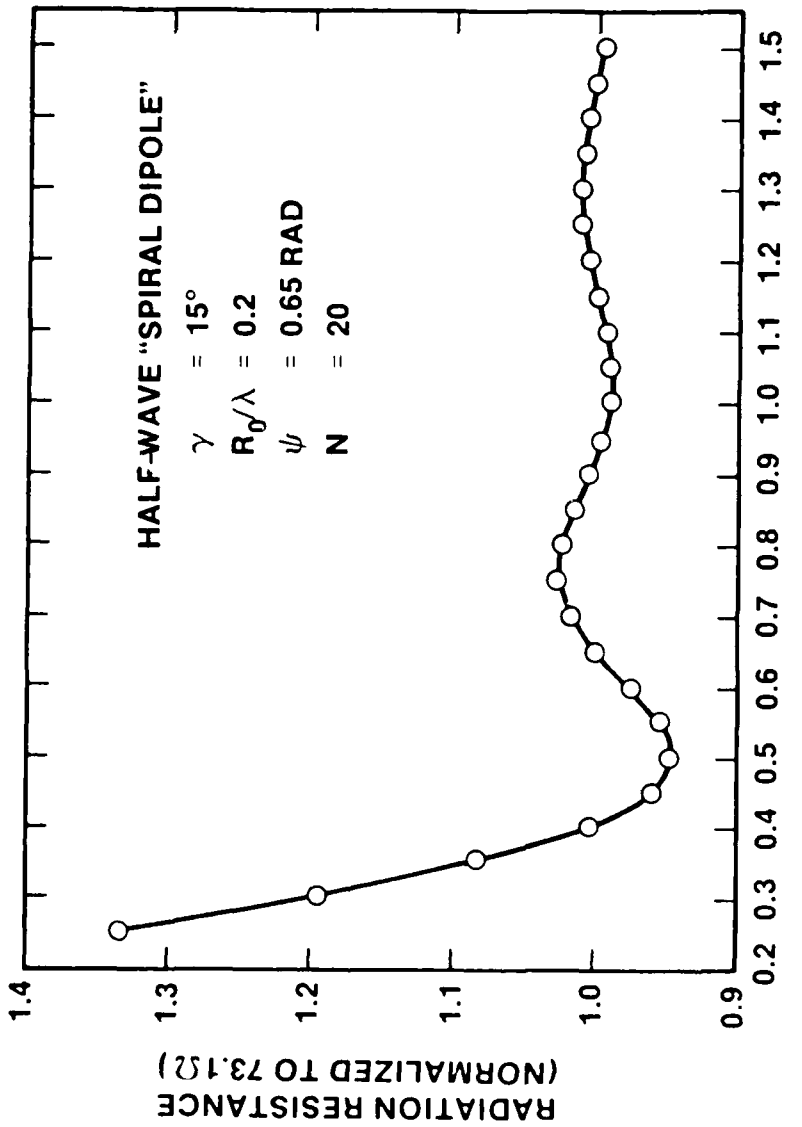

Figure 22. Normalized radiation resistance for half-wave spiral type dipole versus its normalized center height. Inclined 15° from vertical. $R_0/\lambda = 0.2$.

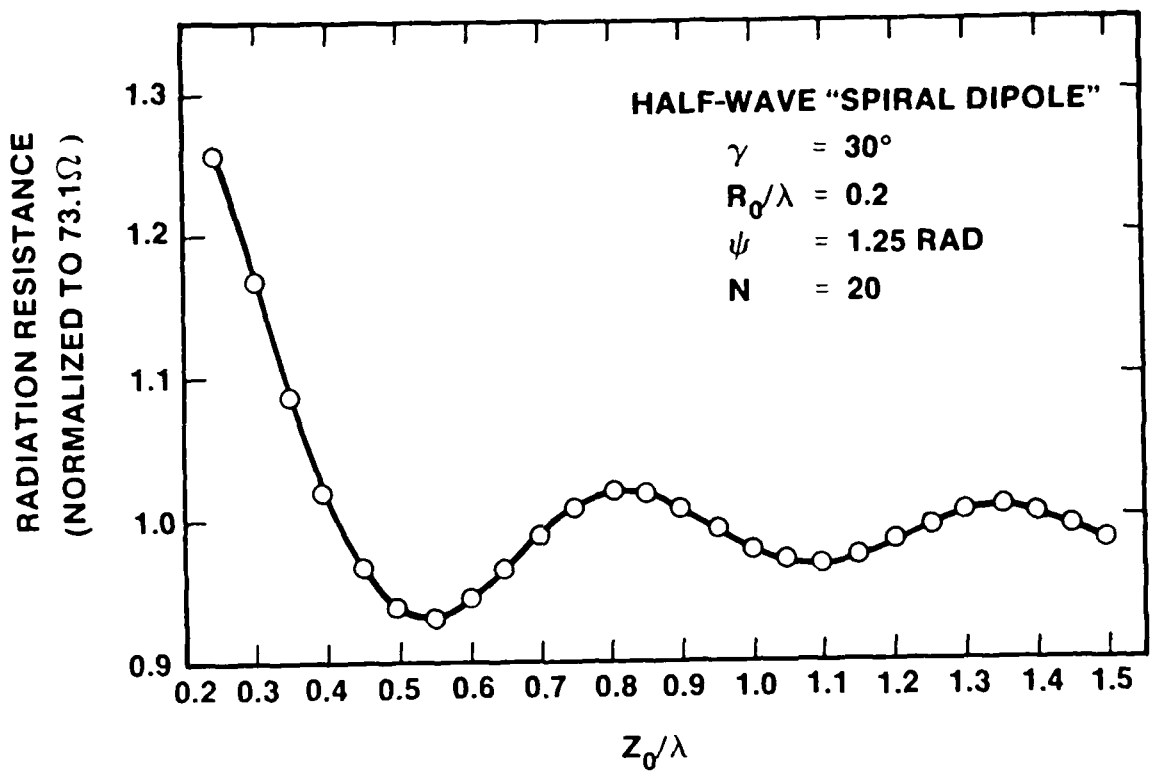

Figure 23. Normalized radiation resistance for half-wave spiral type dipole versus its normalized center height. Inclined 30° from vertical. $R_0/\lambda = 0.2$.

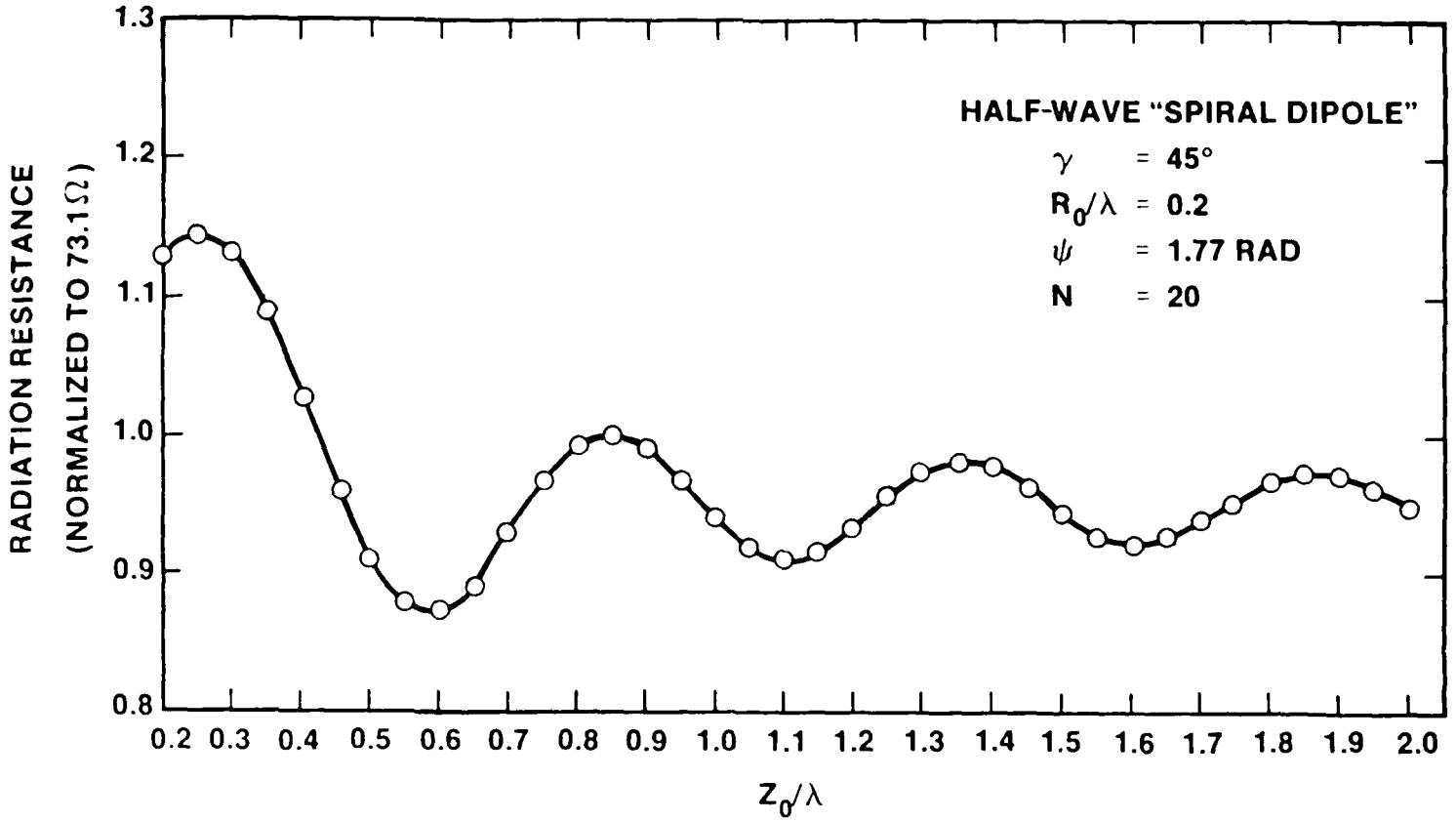

Figure 24. Normalized radiation resistance for half-wave spiral type dipole versus its normalized center height. Inclined 45° from vertical. R_0/λ =0.2.

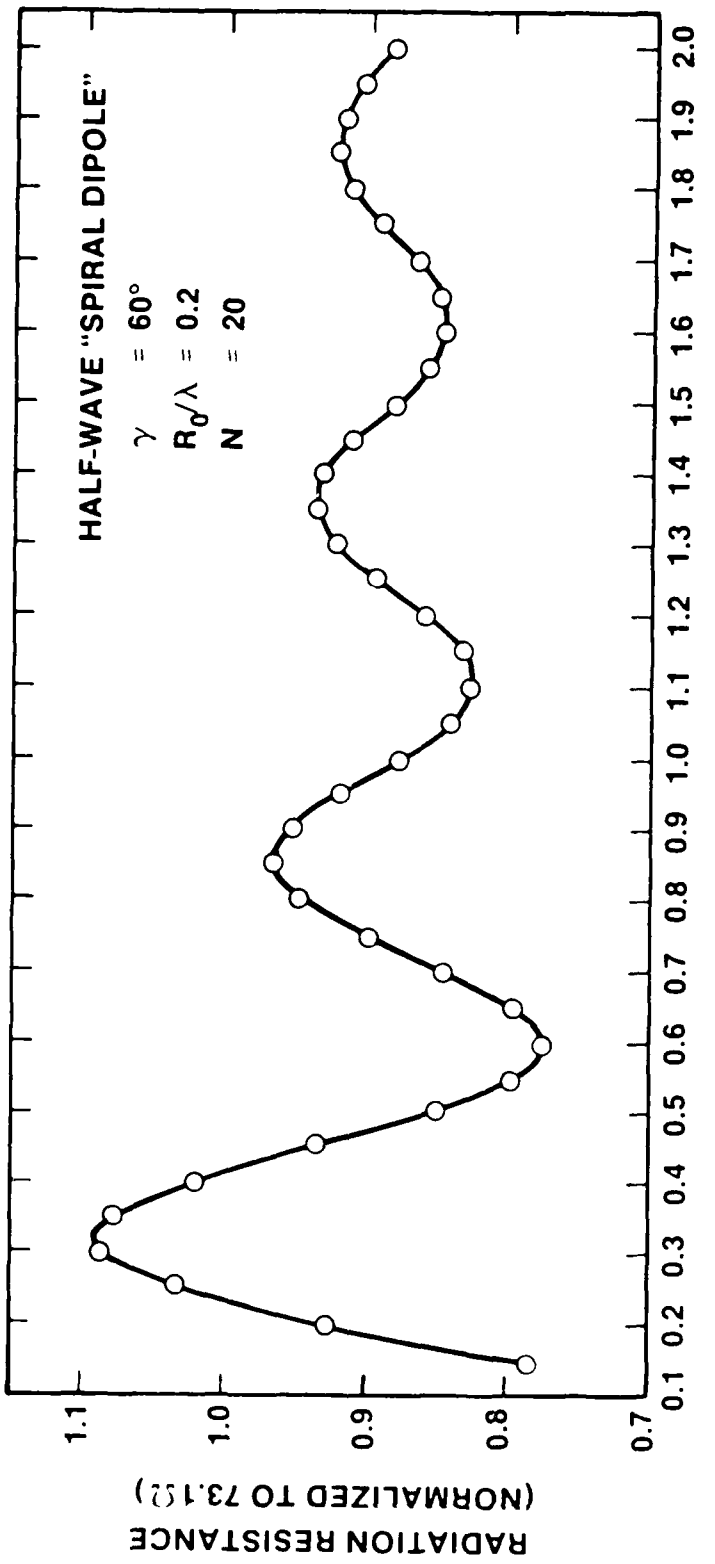

Figure 25. Normalized radiation resistance for half-wave spiral type dipole versus its normalized center height. Inclined 60° from vertical. $R_o/\lambda = 0.2$.

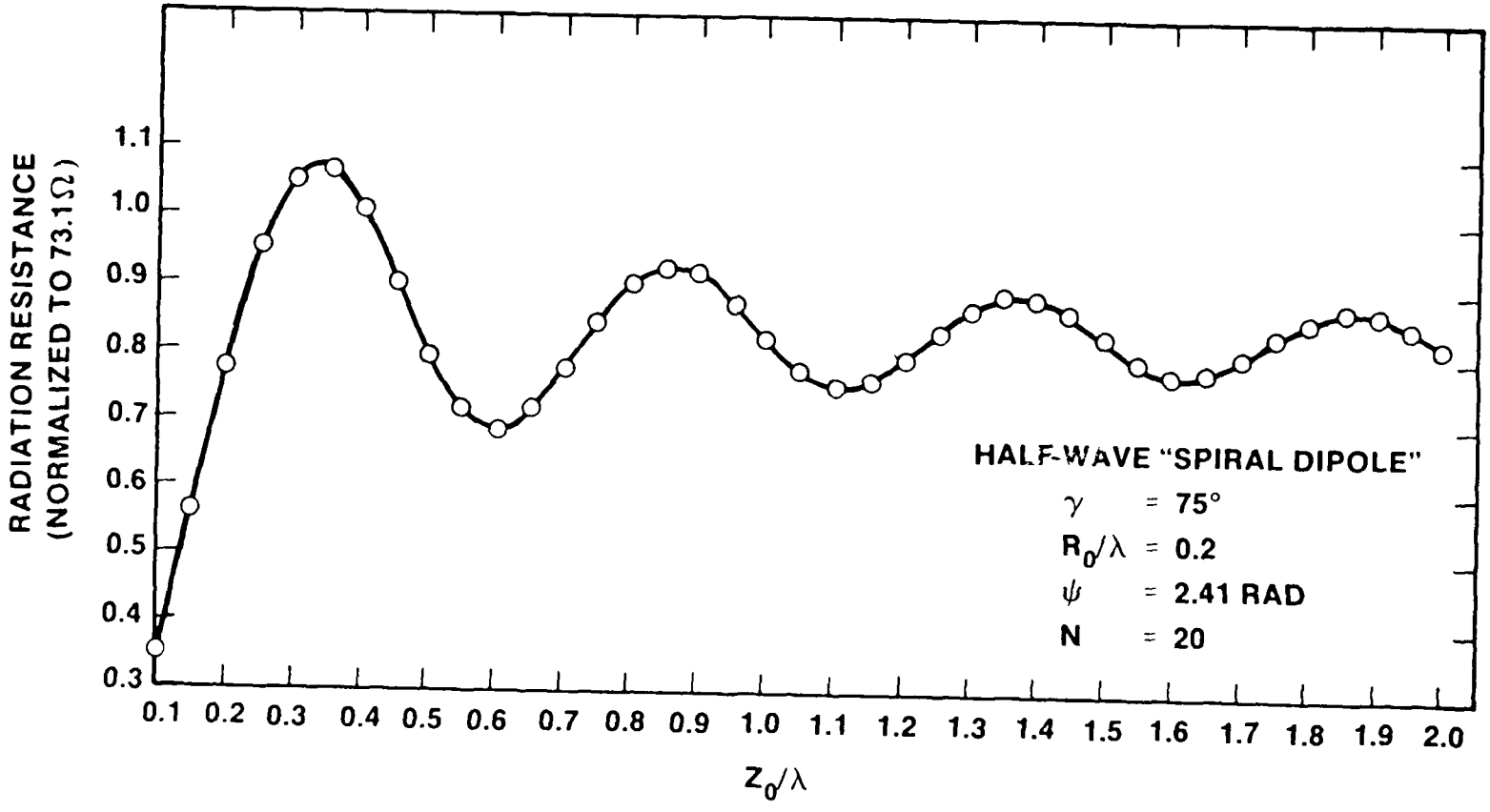

Figure 26. Normalized radiation resistance for half-wave spiral type dipole versus its normalized center height. Inclined 75° from vertical. $R_0/\lambda = 0.2$.

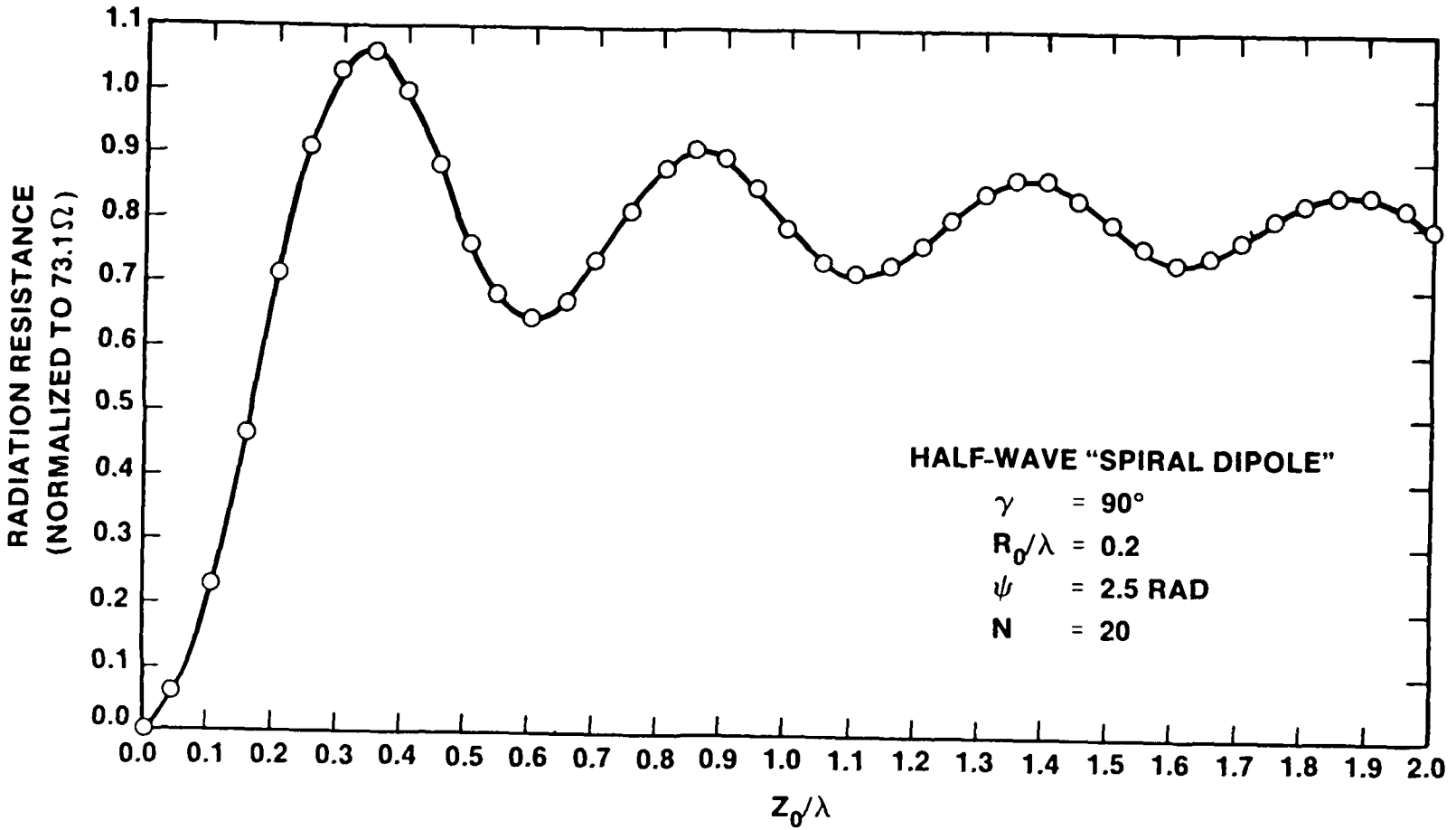

Figure 27. Normalized radiation resistance for half-wave spiral type dipole versus its normalized center height. Partial horizontal loop. $R_0/\lambda = 0.2$.

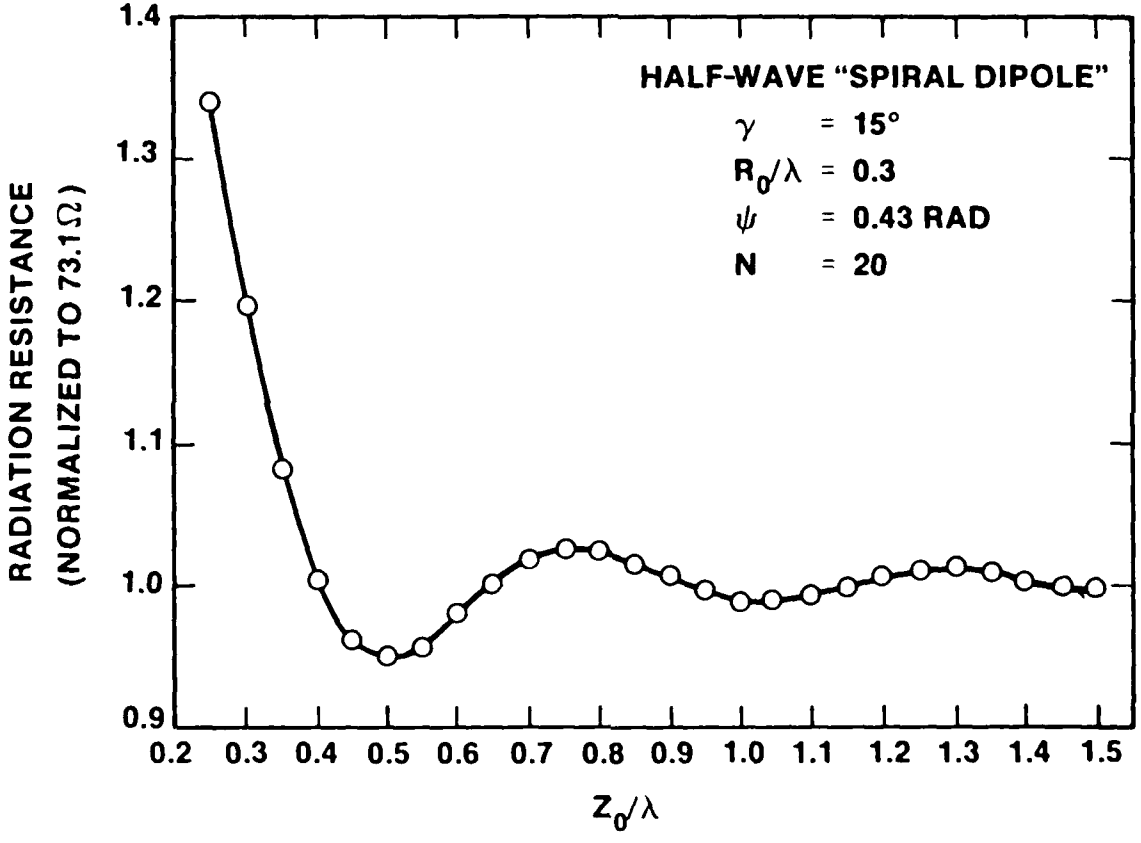

Figure 28. Normalized radiation resistance for half-wave spiral type dipole versus its normalized center height. Inclined 15° from vertical. $R_0/\lambda = 0.3$.

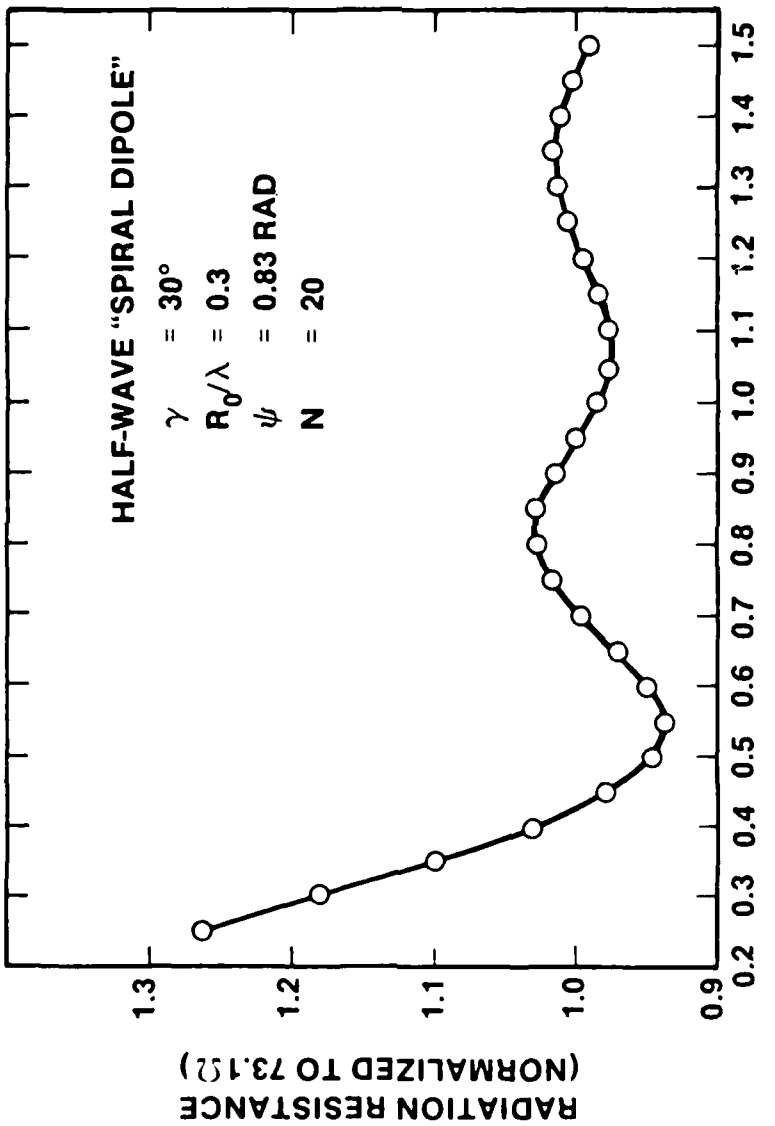

Figure 29. Normalized radiation resistance for half-wave spiral type dipole versus its normalized center height. Inclined 30° from vertical. $R_0/\lambda = 0.3$.

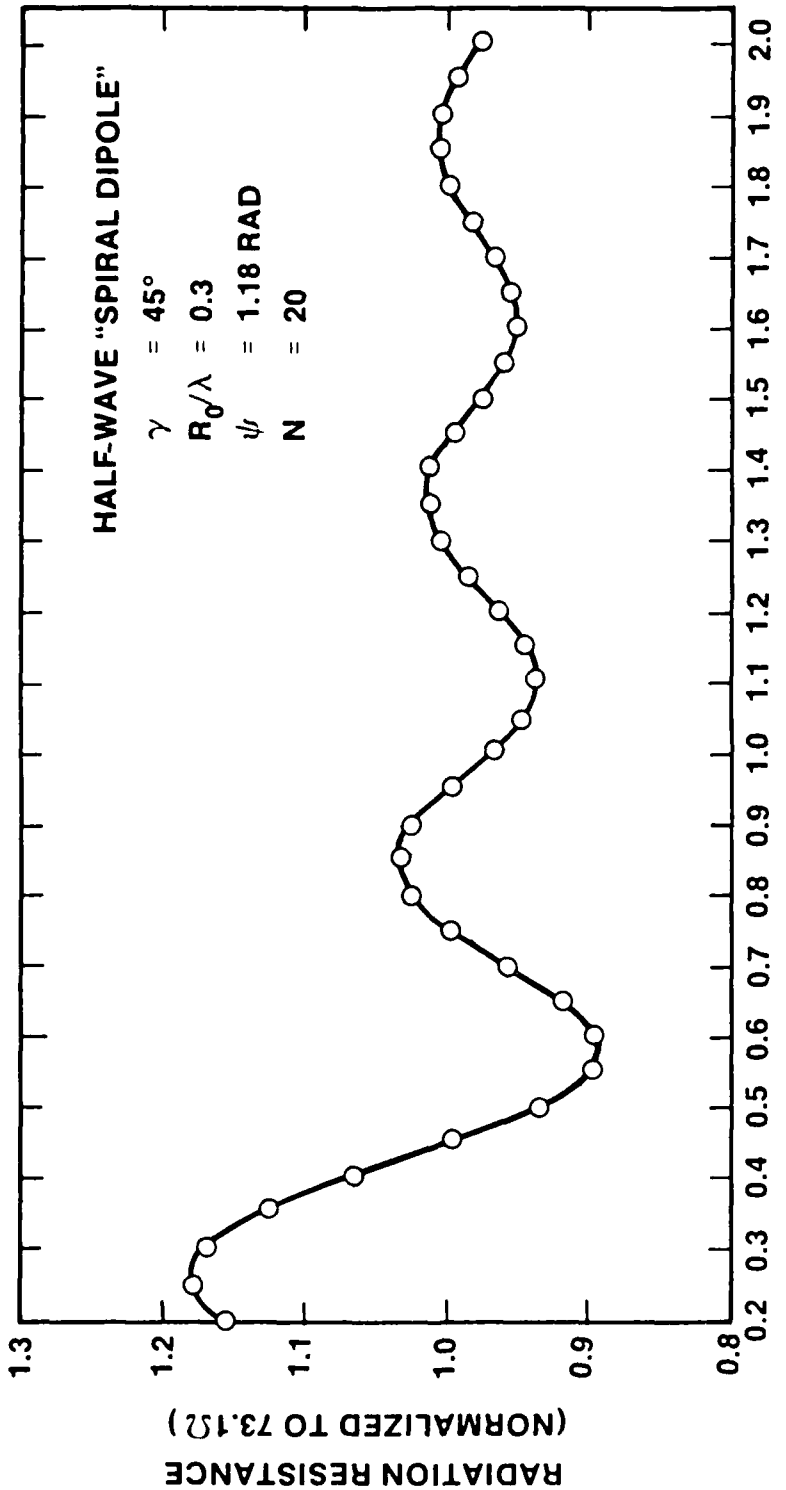

Figure 30. Normalized radiation resistance for half-wave spiral type dipole versus its normalized center height. Inclined 45° from vertical. $R_0/\lambda = 0.3$.

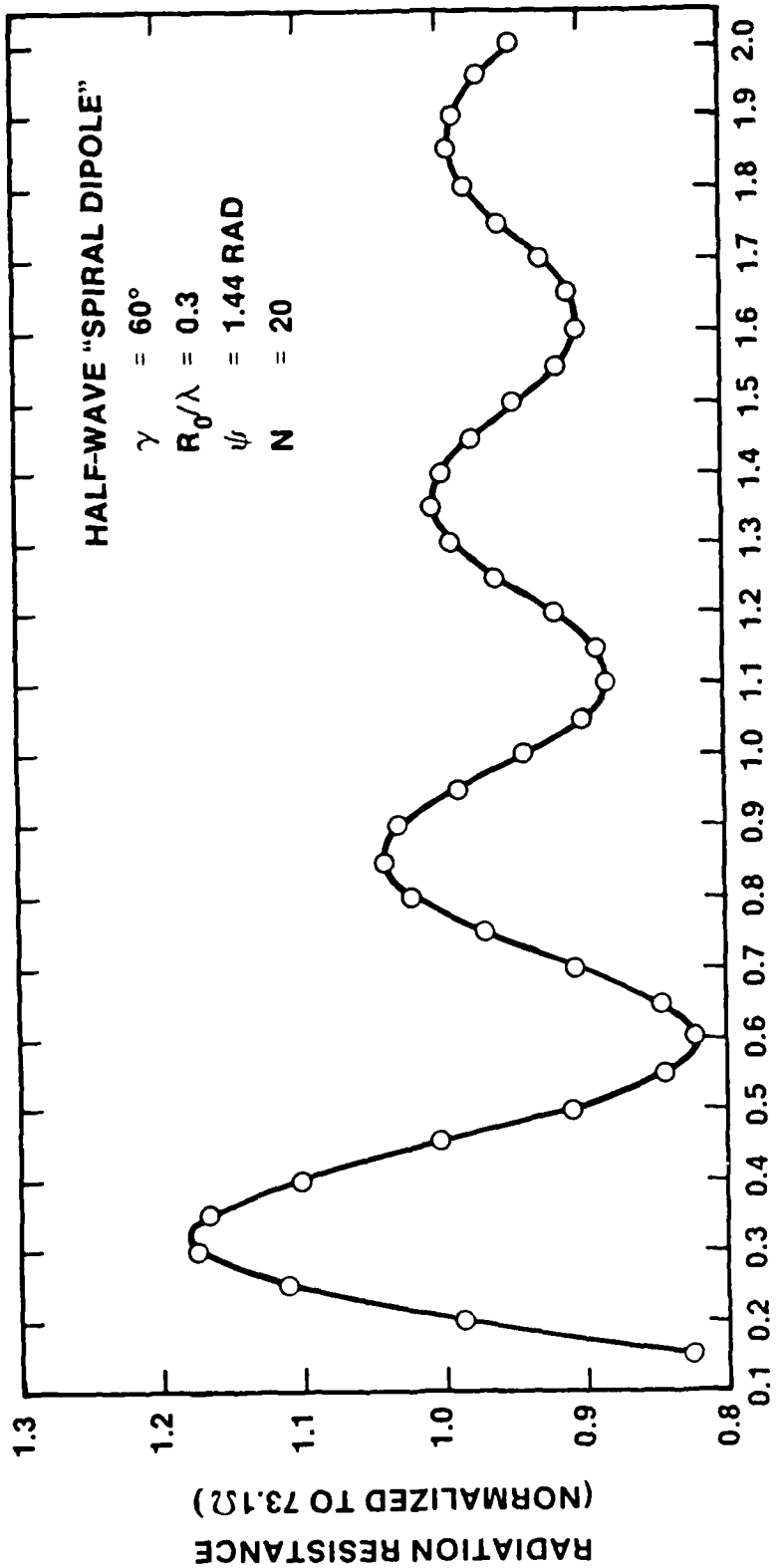

Figure 31. Normalized radiation resistance for half-wave spiral type dipole versus its normalized center height. Inclined 60° from vertical. $R_0/\lambda = 0.3$.

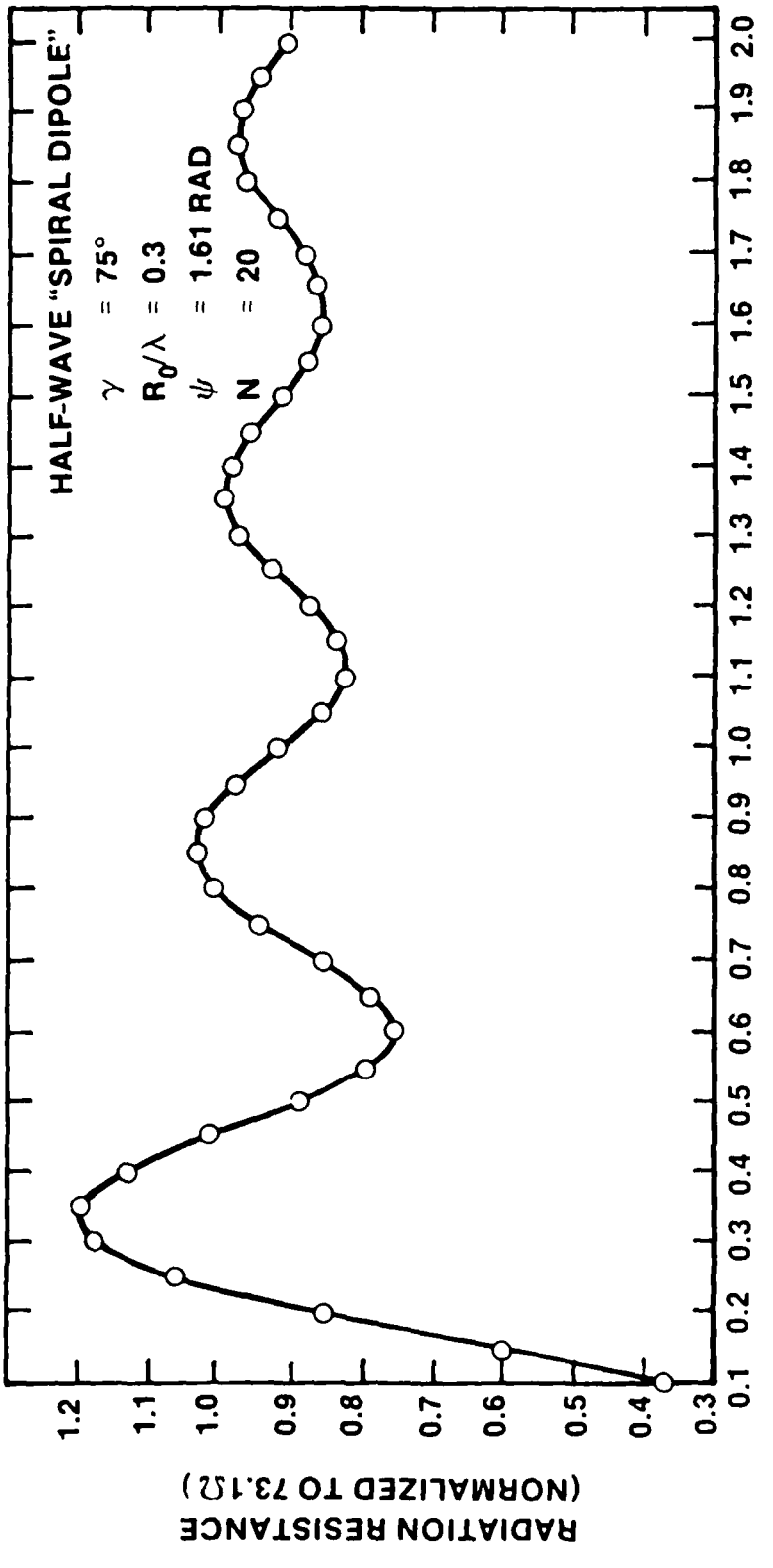

Figure 32. Normalized radiation resistance for half-wave spiral type dipole versus its normalized center height. Inclined 75° from vertical. $R_0/\lambda = 0.3$.

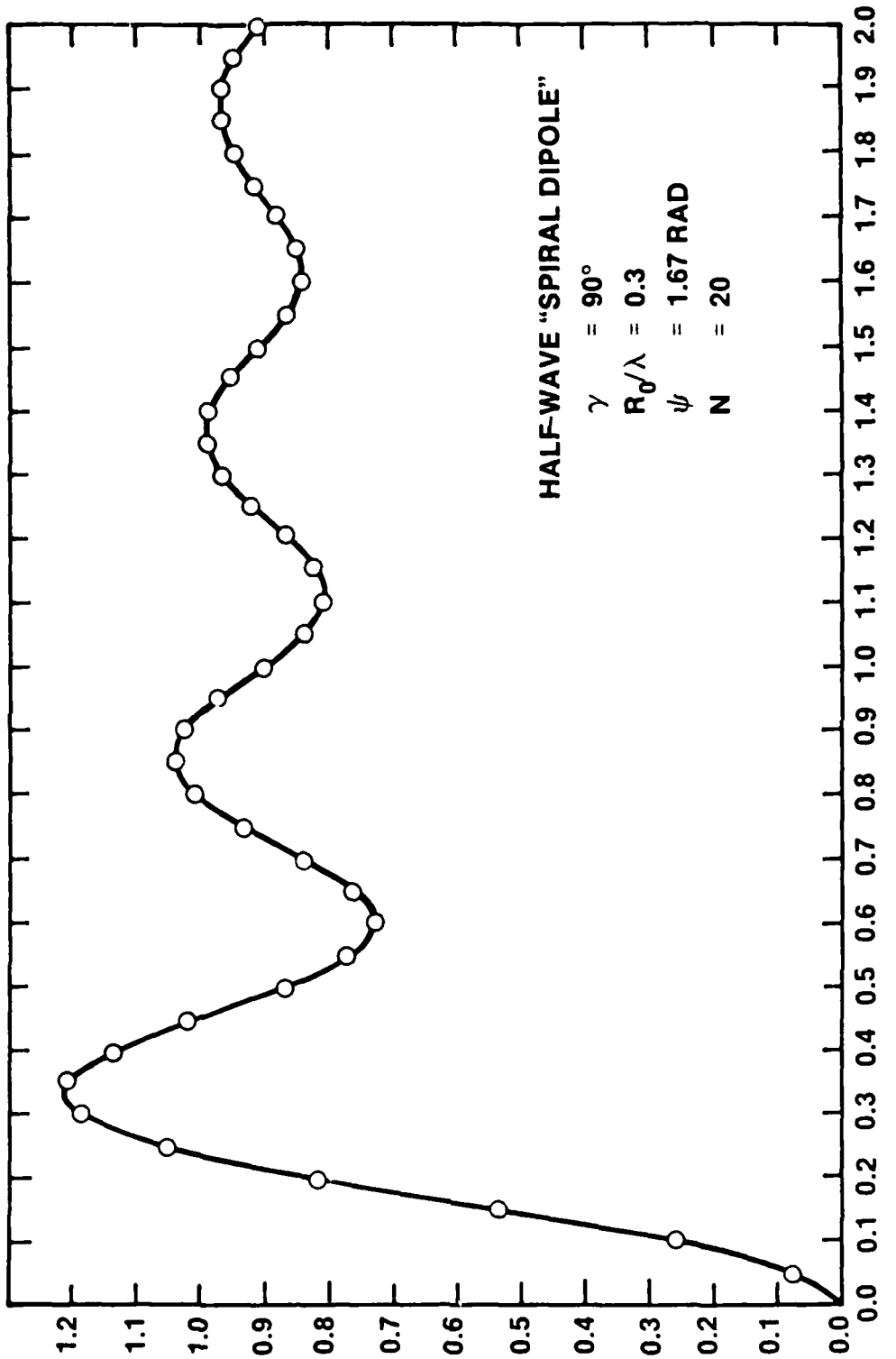

Figure 33. Normalized radiation resistance for half-wave spiral type dipole versus its normalized center height. Partial horizontal loop. $R_0/\lambda = 0.3$.

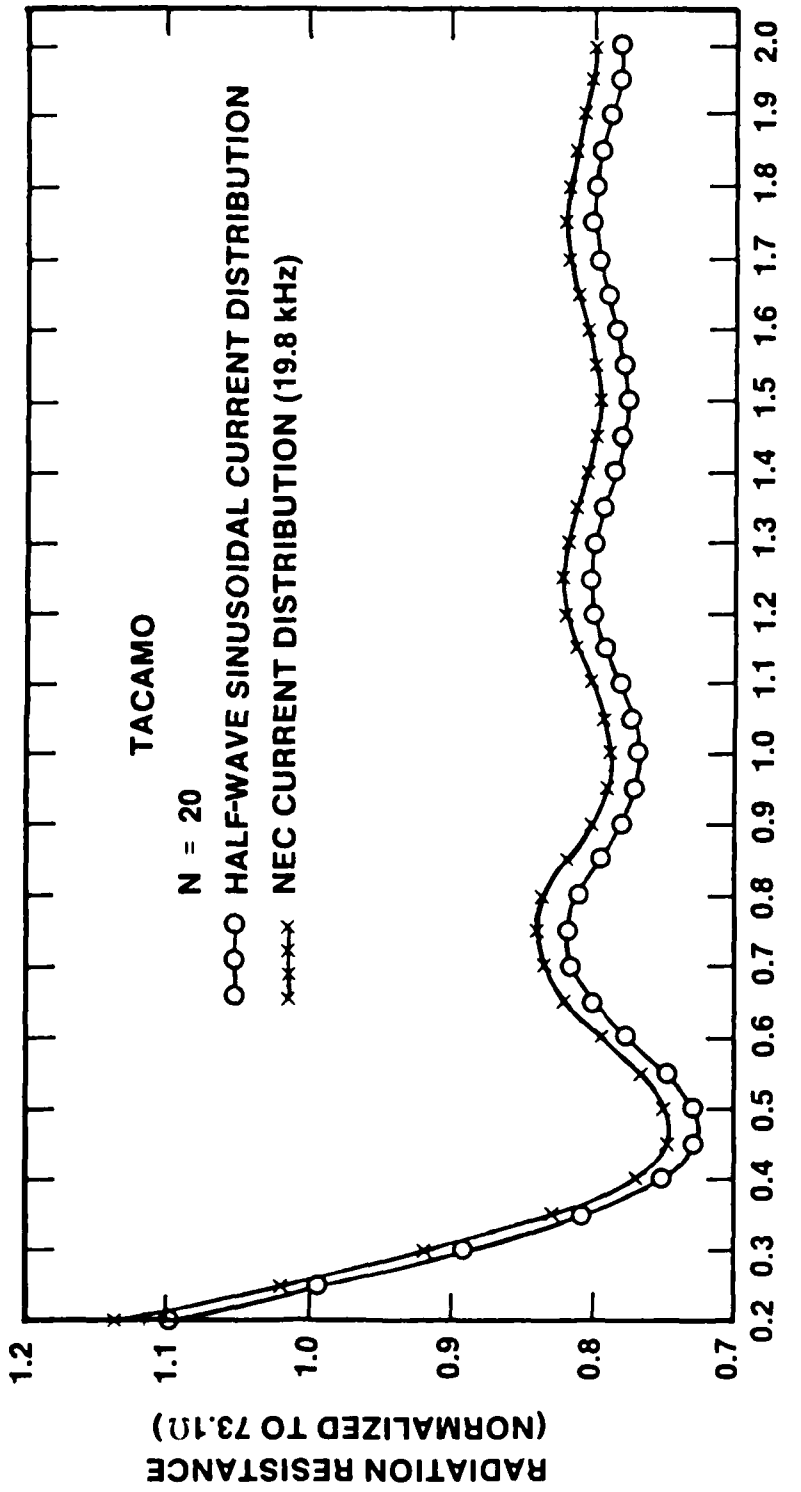

Figure 34. TACAMO 6,000-foot orbit configuration.

DISTRIBUTION LIST

DEPARTMENT OF DEFENSE
DEPUTY UNDER SECRETARY OF DEFENSE
CMD, CONT, COMM & INTELL
DEPARTMENT OF DEFENSE
WASHINGTON, DC 20301

DIRECTOR
COMMAND CONTROL TECHNICAL CENTER
11440 ISAAC NEWTON SQUARE, N
RESTON, VA 22091
C-650

DIRECTOR
COMMAND CONTROL TECHNICAL CENTER
ROOM ME682, THE PENTAGON
WASHINGTON, DC 20301
C-312

DIRECTOR
DEFENSE ADVANCED RESEARCH PROJECT
AGENCY
1440 WILSON BLVD
ARLINGTON, VA 22209
NUCLEAR MONITORING RSCH
STRATEGIC TECH OFFICE

DEFENSE COMMUNICATION ENGINEERING CENTER
1860 WIEHLE AVENUE
RESTON, VA 22090
CODE R220 (M HOROWITZ)
CODE R410
CODE R103

DIRECTOR
DEFENSE COMMUNICATIONS AGENCY
WASHINGTON, DC 20305
CODE 810
CODE 480
CODE 101B

DEFENSE COMMUNICATIONS AGENCY
WWMCCS SYSTEM ENGINEERING ORG
WASHINGTON, DC 20305
RL CRAWFORD

DEFENSE TECHNICAL INFORMATION CENTER
CAMERON STATION
ALEXANDRIA, VA 22314

DIRECTOR
DEFENSE INTELLIGENCE AGENCY
WASHINGTON, DC 20301
DIAST-5
DB-4C (EDWARD O'FARRELL)

DIRECTOR
DEFENSE NUCLEAR AGENCY
WASHINGTON, DC 20305
DDST
TITL TECH LIBRARY
RAAE
STVL

DIRECTOR
JOINT STRAT TGT PLANNING STAFF JCS
OFFUTT AFB
OMAHA, NB 68113
JPST

COMMANDER
FIELD COMMAND
DEFENSE NUCLEAR AGENCY
KIRKTLAND AFB, NM 87115
FCPR

DIRECTOR INTERSERVICE NUCLEAR WEAPONS SCHOOL
KIRTLAND AFB, NM 87115
DOCUMENT CONTROL

CHIEF
LIVERMORE DIVISION FLD COMMAND DNA
LAWRENCE LIVERMORE LABORATORY
PO BOX 808
LIVERMORE, CA 94550
FCPRL

DIRECTOR
NATIONAL SECURITY AGENCY
FT GEORGE G MEADE, MD 20755
W65
OLIVER H BARTLETT W32
TECHNICAL LIBRARY
JOHN SKILLMAN R52

OJCS/J-3
THE PENTAGON
WASHINGTON, DC 20301
OPERATIONS (WWMCCS EVAL
OFF, MR TOMA)

OJCS/J-5
THE PENTAGON
WASHINGTON, DC 20301
PLANS & POLICY (NUCLEAR DIVISION)

UNDER SECRY OF DEFENSE FOR RESEARCH
AND ENGINEERING
DEPARTMENT OF DEFENSE
WASHINGTON, DC 20301
S&SS (OS)

DEPARTMENT OF THE ARMY
COMMANDER/DIRECTOR
ATMOSPHERIC SCIENCES LABORATORY
US ARMY ELECTRONICS COMMAND
WHITE SANDS MISSILE RANGE, NM 88002
DELAS-AE-M (FE NILES)

COMMANDER
HARRY DIAMOND LABORATORIES
2800 POWDER MILL RD
ADELPHI, MD 20783
DELHD-NP (FN WIMENITZ)
MILDRED H WEINER DRXDO-II

COMMANDER
US ARMY NUCLEAR AGENCY
7500 BACKLICK ROAD
BUILDING 2073
SPRINGFIELD, VA 22150
MONA-WE (J BERBERET)

CHIEF
US ARMY RESEARCH OFFICE
PO BOX 12211
TRIANGEL PARK, NC 27709
DRXRD-ZC

DEPARTMENT OF THE NAVY
CHIEF OF NAVAL OPERATIONS
NAVY DEPARTMENT
WASHINGTON, DC 20350
OP 941
OP 604C3
OP 943
OP 981

CHIEF OF NAVAL RESEARCH
NAVY DEPARTMENT
ARLINGTON, VA 22217
CODE 402
CODE 420
CODE 421
CODE 461
CODE 464

COMMANDING OFFICER
NAVAL INTELLIGENCE SUPPORT CENTER
4301 SUITLAND RD BLDG 5
WASHINGTON, DC 20390

OFFICER-IN-CHARGE
WHITE OAK LABORATORY
NAVAL SURFACE WEAPONS CENTER
SILVER SPRING, MD 20910
CODE WA501 NAVY NUC PRGMS OFF
CODE WX21 TECH LIBRARY

COMMANDER
NAVAL TELECOMMUNICATIONS COMMAND
NAVTELCOM HEADQUARTERS
4401 MASSACHUSETTS AVE, NW
WASHINGTON, DC 20390
CODE 24C

COMMANDING OFFICER
NAVY UNDERWATER SOUND LABORATORY
FORT TRUMBULL
NEW LONDON, CT 06320
PETER BANNISTER
DA MILLER

DIRECTOR
STRATEGIC SYSTEMS PROJECT OFFICE
NAVY DEPARTMENT
WASHINGTON, DC 20376
N141

DEPARTMENT OF THE AIR FORCE
COMMANDER
ADC/DC
ENT AFB, CO 80912
DC (MR LONG)

COMMANDER
ADCOM/XPD
ENT AFB, CO 80912
XPQDQ
XP

AF GEOPHYSICS LABORATORY, AFSC
HASCOM AFB, MA 01731
CRU (S HOROWITZ)

AF WEAPONS LABORATORY, AFSC
KIRTLAND AFB, NM 87117
SUL (2)
DYC

COMMANDER
ROME AIR DEVELOPMENT CENTER, AFSC
GRIFFISS AFB, NY 13440
EMTLD DOC LIBRARY

COMMANDER
ROME AIR DEVELOPMENT CENTER, AFSC
HANSCOM AFB, MA 01731
EEP JOHN RASMUSSEN

COMMANDER IN CHIEF
STRATEGIC AIR COMMAND
OFFUTT AFB, NB 68113
NRT
XPFS

LAWRENCE LIVERMORE NATIONAL
LABORATORY
PO BOX 808
LIVERMORE, CA 94550
TECH INFO DEPT L-3

LOS ALAMOS NATIONAL SCIENTIFIC
LABORATORY
PO BOX 1663
LOS ALAMOS, NM 87545
DOC CON FOR TF TASCHEK
DOC CON FOR D R WESTERVELT
DOC CON FOR PW KEATON

SANDIA LABORATORY
LIVERMORE NATIONAL LABORATORY
PO BOX 969
LIVERMORE, CA 94550
DOC CON FOR BE MURPHEY
DOC CON FOR TB COOK ORG 8000

SANDIA NATIONAL LABORATORY
PO BOX 5800
ALBUQUERQUE, NM 87115
DOC CON FOR SPACE PROJ DIV
DOC CON FOR AD THORNBROUGH
DOC CON FOR 3141 SANDIA RPT COLL

OTHER GOVERNMENT
DEPARTMENT OF COMMERCE
NATIONAL BUREAU OF STANDARDS
WASHINGTON, DC 20234
RAYMOND T MOORE

DEPARTMENT OF COMMERCE
OFFICE OF TELECOMMUNICATIONS
INSTITUTE FOR TELECOM SCIENCE
BOULDER, CO 80302
WILLIAM F UTLAUT
LA BERRY
A GLENN JEAN

DEPARTMENT OF DEFENSE CONTRACTORS
AEROSPACE CORPORATION
PO BOX 92957
LOS ANGELES, CA 90009
IRVING M GARFUNKEL

ANALYTICAL SYSTEMS ENGINEERING CORP
5 OLD CONCORD RD
BURLINGTON, MA 01803
RADIO SCIENCES

THE BOEING COMPANY
PO BOX 3707
SEATTLE, WA 98124
GLENN A HALL
JF KENNEY

ESL, INC
495 JAVA DRIVE
SUNNYVALE, CA 94086
JAMES MARSHALL

GENERAL ELECTRIC COMPANY
SPACE DIVISION
VALLEY FORGE SPACE CENTER
GODDARD BLVD KING OF PRUSSIA
PO BOX 8555
PHILADELPHIA, PA 19101
SPACE SCIENCE LAB (MH BORTNER)

KAMAN TEMPO
816 STATE STREET
PO DRAWER QQ
SANTA BARBARA, CA 93102
B GAMBILL
DASIAC
WARREN S KNAPP

GTE SYLVANIA, INC
ELECTRONICS SYSTEMS GRP
EASTERN DIVISION
77 A STREET
NEEDHAM, MA 02194
MARSHAL CROSS

ITT RESEARCH INSTITUTE
10 WEST 35TH STREET
CHICAGO, IL 60616
TECHNICAL LIBRARY

UNIVERSITY OF ILLINOIS
DEPARTMENT OF ELECTRICAL ENGINEERING
URBANA, IL 61803
AERONOMY LABORATORY

JOHNS HOPKINS UNIVERSITY
APPLIED PHYSICS LABORATORY
JOHNS HOPKINS ROAD
LAUREL, MD 20810
J NEWLAND
PT KOMISKE

LOCKHEED MISSILE & SPACE CO, INC.
3251 HANOVER STREET
PALO ALTO, CA 94304
EE GAINES
WL IMHOF D/52-12
JB REAGAN D652-12
RG JOHNSON D/52-12

MASSACHUSETTS INSTITUTE OF TECHNOLOGY
LINCOLN LABORATORY
PO BOX 73
LEXINGTON, MA 02173
DM TOWLE

MISSION RESEARCH CORPORATION
735 STATE STREET
SANTA BARBARA, CA 93101
R HENDRICK
F FAJEN

PACIFIC-SIERRA RESEARCH CORP
12340 SANTA MONICA BLVD.
LOS ANGELES' CA 90025
EC FIELD, JR

PENNSYLVANIA STATE UNIVERSITY
IONOSPHERIC RESEARCH LABORATORY
318 ELECTRICAL ENGINEERING EAST
UNIVERSITY PARK, PA 16802
IONOSPHERIC RSCH LAB

R&D ASSOCIATES
PO BOX 9695
MARINA DEL REY, CA 90291
FORREST GILMORE
WILLIAM J KARZAS
PHYLLIS GREIFINGER
CARL GREIFINGER
HA ORY
BRYAN GABBARD
RP TURCO
SAUL ALTSCHULER

RAND CORPORATION
1700 MAIN STREET
SANTA MONICA, CA 90406
TECHNICAL LIBRARY
CULLEN CRAIN

SRI INTERNATIONAL
333 RAVENSWOOD AVENUE
MENLO PARK, CA 94025
DONALD NEILSON
GEORGE CARPENTER
WG CHETNUT
JR PETERSON
GARY PRICE

STANFORD UNIVERSITY
RADIO SCIENCE LABORATORY
STANFORD, CA 94305
RA HELLIWELL
FRASER SMITH
J KATSUFRAKIS

CALIFORNIA INSTITUTE OF TECHNOLOGY
JET PROPULSION LABORATORY
4800 OAK GROVE DRIVE
PASADENA, CA 91103
ERNEST K SMITH

END

DTIC

9-86